REPORT DOCUMENTATION PAGE

Form Approved OMB NO. 0704-0188

1. REPORT DATE (DD-MM-YYYY)	2. REPORT TYPE	3. DATES COVERED (From - To)
16-03-2011	Final Report	1-Oct-2008 - 30-Sep-2010

4. TITLE AND SUBTITLE
Army - UNL Center for Trauma Mechanics

5a. CONTRACT NUMBER
W911NF-08-1-0483

5b. GRANT NUMBER

5c. PROGRAM ELEMENT NUMBER
622105

6. AUTHORS
Dr. Namas Chandra, Dr. Ruqiang Feng, Dr. C. A. Nelson, Dr. Jung Yul Lim, Dr. Joseph A. Turner, Dr. Florin Bobaru, Dr. Mehrdad Negahban

5d. PROJECT NUMBER

5e. TASK NUMBER

5f. WORK UNIT NUMBER

7. PERFORMING ORGANIZATION NAMES AND ADDRESSES
University of Nebraska
Research Grants & Contracts
303 Administration Bldg.
Lincoln, NE 68588 -0430

8. PERFORMING ORGANIZATION REPORT NUMBER

9. SPONSORING/MONITORING AGENCY NAME(S) AND ADDRESS(ES)
U.S. Army Research Office
P.O. Box 12211
Research Triangle Park, NC 27709-2211

10. SPONSOR/MONITOR'S ACRONYM(S)
ARO

11. SPONSOR/MONITOR'S REPORT NUMBER(S)
55136-EG.1

12. DISTRIBUTION AVAILIBILITY STATEMENT
Approved for Public Release; Distribution Unlimited

13. SUPPLEMENTARY NOTES
The views, opinions and/or findings contained in this report are those of the author(s) and should not contrued as an official Department of the Army position, policy or decision, unless so designated by other documentation.

14. ABSTRACT
The goal of this project is to understand the fundamental material and mechanical behaviors of protective systems in mitigating brain trauma under blast loading conditions.Such knowledge will enable the development of a reliable, repeatable testbed to validate new protective systems under blast loading conditions and, subsequently, reduce the short- and long-term effects of blast waves on the warfighter.This project will employ novel sensor, imaging, and engineering technologies to quantitatively characterize the mechanics of mild blast-induced traumatic

15. SUBJECT TERMS
RED Head (Realistic Explosive Dummy Head) Development, Effects of Impulsive Pressurization on Brain Cell Functions: blast-induced traumatic brain injury (bTBI)

16. SECURITY CLASSIFICATION OF:			17. LIMITATION OF ABSTRACT	15. NUMBER OF PAGES	19a. NAME OF RESPONSIBLE PERSON
a. REPORT	b. ABSTRACT	c. THIS PAGE			Namas Chandra
UU	UU	UU	UU		19b. TELEPHONE NUMBER: 402-472-8310

Standard Form 298 (Rev 8/98)
Prescribed by ANSI Std. Z39.18

Report Title

Army - UNL Center for Trauma Mechanics

ABSTRACT

The goal of this project is to understand the fundamental material and mechanical behaviors of protective systems in mitigating brain trauma under blast loading conditions.Such knowledge will enable the development of a reliable, repeatable testbed to validate new protective systems under blast loading conditions and, subsequently, reduce the short- and long-term effects of blast waves on the warfighter.This project will employ novel sensor, imaging, and engineering technologies to quantitatively characterize the mechanics of mild blast-induced traumatic brain injury (mbTBI) and the resulting neuronal injury thresholds in cellular and small animal models, headform models, and post-mortem human specimens (PMHS).The development of efficacious protective measures against blast-induced shockwaves is critical to decrease the incidence and long-term effects of mbTBI among the nation's warfighters.This project is underpinned by four research objectives:

1. Determine how blast waves interact with the skull and cranium prior to entering the brain.
2. Identify the role of protective helmets in influencing the relationship between an externally applied blast wave and the corresponding internal state of stress, pressure, or deformation.
3. Create reliable bio-fidelic models using small animal models, PMHS, and numerical simulations that can mimic battlefield conditions.
4. Develop neuron injury models and relate injury to external loads through experiments and simulations.

List of papers submitted or published that acknowledge ARO support during this reporting period. List the papers, including journal references, in the following categories:

(a) Papers published in peer-reviewed journals (N/A for none)

. G. Cao and Chandra, N. Evaluating the Biological Cell Properties Using Dynamic Indentation Method, Physical Review E, 81, 021924, 1-9, (2010).

• Goel*, M. Negahban, L. Zhang*, "Modeling nonlinear thermo-elastic response for glassy polycarbonate using ultrasonic results under compression in a confined cell," Mechanics of Materials (doi:10.1016/j.mechmat.2011.02.006).

• L. Zhang*, T. Boulet*, J. Hein*, M. Arnoult, M. Negahban, "Material characterization and modeling of head for dynamic simulations," Proceedings of the ICCES'10, Los Vegas, NV, March 28-April 1, 2010.

Number of Papers published in peer-reviewed journals: 3.00

(b) Papers published in non-peer-reviewed journals or in conference proceedings (N/A for none)

1. Matthew Nienaber,* Jeong Soon Lee,* Ruqiang Feng, Jung Yul Lim. Impulsive pressurization of neuronal cells for traumatic brain injury study. J. Vis. Exp. submitted (*: contributed equally).
2. G. Sailesh, L. Gu, G. Cao and Chandra, N. Role of Helmet on Mitigating the Blast Induced Injury, ASME International Mechanical Engineering Congress and Exposition (IMECE09), Lake Buena Vista, Florida, November 2009.
3. G. Cao and N. Chandra, Substrate Effect on Dynamic Indendation Measurement of Biological Cell Properties, Materials Research Society (MRS) Spring Conference, San Francisco, California, April 2009.

Number of Papers published in non peer-reviewed journals: 3.00

(c) Presentations

1. G, Cao, Y. Zhou, J.S. Lee, J.Y. Lim, and N. Chandra, Mechanical Model of Neuronal Function Loss, 16th US National Congress of Theoretical and Applied Mechanics (USNCTAM2010), State College, PA June 27-July 2, 2010
2. G. Cao and N. Chandra, Evaluating the Mechanical Behavior of Biological Cell Based on Scanning Probe Indentation, the 3rd International Conference on Mechanics of Biomaterials & Tissues (ICMOBT), Clear Water Beach, Florida, December, 2009.
3. G. Cao and N. Chandra, Evaluating the Nucleus Effect on the Cell Mechanical Behavior, 2009 ASME International Mechanical Engineering Congress and Exposition (IMECE09), Lake Buena Vista, Florida, November, 2009.
4. G. Shailesh, G. Cao and N. Chandra, Computational Simulation of the Helmet Effect on the Blast Induced Traumatic Brain Injury, 10th U.S. National Congress on Computational Mechanics, Columbus, Ohio, July, 2009.
5. G. Shailesh, L. Gu, G. Cao and N. Chandra, The Effect of Shock Wave on a Human Head, 2009 ASME International Mechanical Engineering Congress and Exposition (IMECE09), Lake Buena Vista, Florida, November 13-19, 2009.
6. Ganpule, S. Gu. L.X. and Chandra, N, Modeling Shock Response of Human Head Using Fluid-Structure Interaction (FSI), 16th US National Congress of Theoretical and Applied Mechanics (USNCTAM2010), State College, PA June 27-July 2, 2010
7. Ganpule, S. Gu. L.X. and Chandra, N, MRI-Based Three Dimensional Modeling of Blast Traumatic Brain Injury, 2010 ASME International Engineering Congress and RD&D Expo, Vancouver, British Columbia, Canada November 12-18, 2010
8. Ganpule, S., Gu, L.X and Chandra N., Role of Helmet in Mitigating Traumatic Brain Injury, BMES Annual Fall Meeting: Bridging Biology, Engineering and Medicine, Pittsburgh, PA, October 7-10, 2009
9. J. Hein*, B. McMichen*, A. Stibbe*, M. Negahban, D. Cullen, J. Turner, M. Akhter "Mapping tibial surface strains using 3D stereo optical system," 47th Annual Technical Meeting of Society of Engineering Science, Iowa State University, Ames, IA, 3-6 October, 2010.
10. J. Hein*, B. McMichen*, A. Stibbe*, M. Negahban, D. Cullen, J. Turner, M. Akhter, "Mapping tibial surface strains using 3D stereo optical system," (poster) ASBMR 2010 Annual Meeting, Toronto, Canada, October 16-18, 2010.
11. Jeong Soon Lee, Matthew Nienaber, Ruqiang Feng, Jung Yul Lim. Impulsive pressurization of neuronal cells for studying traumatic brain injury. 2010 Biomedical Engineering Society (BMES), #PS-9A-11-142, October 6-9, 2010, Austin, TX, USA.
12. K. Strabala*, L. Delbreilh*, J.-M. Saiter, M. Negahban "Effects of compression and aging on the fracture, mechanical, and thermal properties of glassy polycarbonate," 17thWorld Forum on Advanced Materials (PolyChar 17), Rouen, France, April 20-24, 2009.
13. L Zhang*, T. Boulet*, J. Hein*, M. Negahban, "Material Characterization and Modeling of Head for Dynamic Simulations," International Conference on Computational & Experimental Engineering and Sciences, ICCEES'10, Las Vegas, USA, March 28-Aprpril 1, 2010.
14. L. Zhang*, M. Negahban "Wave prorogations in pre-deformed nonlinear viscoelastic materials," 47th Annual Technical Meeting of Society of Engineering Science, Iowa State University, Ames, IA, 3-6 October, 2010.
15. M. Negahban, A. Goel*, K. Strabala*, J. Vogeler*, R. Feng, "Experimental characterization and constitutive modeling of polycarbonate under change of temperature, strain and strain rate," 17th World Forum on Advanced Materials (PolyChar 17), Rouen, France, April 20-24, 2009.
16. M. Negahban, A. Goel, K. Strabala*, "The role of evolving anisotropy in modeling the small and large deformation thermodynamic viscoealstic and viscoplastic response of glassy polymers," 7th International Conference on Mechanics of Time-Dependent Materials, Portoroz, Slovenia, September 5-11, 2010.
17. M. Negahban, A. Goel, L. Zhang*, K. Strabala*, Q. Fichot*, F. Souza, S. Meagher*, J. A. Turner, D. Allen, et L. Delbreilh, "Characterization, Modeling, and Consequences of the Development During Plastic Flow of Large Anisotropy in the Wave-Speeds and Fracture," in New Models and Hydrocodes for Shock Wave Processes, Paris, France, 24-28 May, 2010.
18. M. Negahban, A. Goel, L. Zhang*, K. Strabala*, Q. Fichot*, F. Souza, S. Meagher*, J. A. Turner, D. Allen, J.-M. Saiter, L. Delbreilh, "Plasticity-like modeling of nonlinear viscoelastic response and its application to glassy polymers and biological tissue," Composites and Infrastructures Workshop, Verese, Italy, May, 2010.
19. Matthew Nienaber, Jeong Soon Lee, Ruqiang Feng, Jung Yul Lim. Impulsive pressurization of neuronal cells. 47th Annual Technical Meeting of Society of Engineering Science, October 4-6, 2010, Ames, IA, USA.
20. N. Chandra, Micromechanical Injury Threshold Models of Neurons-Experiments and Theory, DOD Brain Injury Computational Modeling Expert Panel Meeting, St. Pete Beach, Florida, August 2010.
21. Namas Chandra, Trauma Mechanics Research: Helmet design, brain and skull modeling, UNL Pentagon Research meeting, 28 July, 2010.
22. S. G. M. Hossain, C. A. Nelson, T. Boulet, M. Arnoult, L. Zhang, A. Holmberg, J. Hein, N. Kleinschmit, E. Sogbesan, 2010, "Material Modeling and Development of a Realistic Dummy Head for Testing Blast Induced Traumatic Brain Injury," IV European Conference on Computational Mechanics – ECCM 2010, Paris.
23. S. G. M. Hossain, C. A. Nelson, T. Boulet, M. Arnoult, L. Zhang, A. Holmberg, J. Hein, N. Kleinschmit, E. Sogbesan, 2010, "Material Modeling and Development of a Realistic Dummy Head for Testing Blast Induced Traumatic Brain Injury," IV European Conference on Computational Mechanics – ECCM 2010, Paris.
24. S. Meagher*, K. Strabala*, C. Landais*, L. Delbreilh, M. Negahban, J. Turner, "Anomalous Loss of Toughness with Physical Aging of Work Toughened Polycarbonate," 47th Annual Technical Meeting of Society of Engineering Science, Iowa State University, Ames, IA, 3-6 October, 2010.

25. S.G.M. Hossain, Mickael Arnoult, Thomas Boulet, Charles Landais, Jonathan Hein and Carl Nelson, 2010, "Material Analysis for the Development of a Surrogate Headform to be Tested Under Blast-Induced Shock Loading," Abstracts, Society of Engineering Science 47th Annual Technical Meeting, Ames, IA.
26. S.G.M. Hossain, Mickael Arnoult, Thomas Boulet, Charles Landais, Jonathan Hein and Carl Nelson, 2010, "Material Analysis for the Development of a Surrogate Headform to be Tested Under Blast-Induced Shock Loading," Abstracts, Society of Engineering Science 47th Annual Technical Meeting, Ames, IA.
27. Youn Doh Ha, Shailesh Ganpule, Florin Bobaru, and Ruqiang Feng, "Fluid-structure interaction models of air blast on head," SES 2010 (47th Annual Technical Meeting of Society of Engineering Science), Iowa state university, Ames, IA, Oct.3-6, 2010.
28. Aaron Holmberg, Nicholas N. Kleinschmit, Ruqiang Feng, Youn Doh Ha, and Florin Bobaru, "Shock-tube-simulated blast wave propagation and interactions with solid structures," SES 2010 (47th Annual Technical Meeting of Society of Engineering Science), Iowa state university, Ames, IA, Oct.3-6, 2010.

Number of Presentations: 28.00

Non Peer-Reviewed Conference Proceeding publications (other than abstracts):

Number of Non Peer-Reviewed Conference Proceeding publications (other than abstracts): 0

Peer-Reviewed Conference Proceeding publications (other than abstracts):

Number of Peer-Reviewed Conference Proceeding publications (other than abstracts): 0

(d) Manuscripts

Matthew Nienaber,* Jeong Soon Lee,* Ruqiang Feng, Jung Yul Lim. Impulsive pressurization of neuronal cells for traumatic brain injury study. J. Vis. Exp. submitted (*: contributed equally).

Number of Manuscripts: 1.00

Patents Submitted

Patents Awarded

Awards

Dr. C.A.Nelson:
UNL ME Department 2008-09 Teaching Award.
UNL College of Engineering Henry Y. Kleinkauf Family Distinguished New Faculty Teaching Award, 4/10.
UNL Pi Tau Sigma Golden Key Award 2009-2010, Outstanding Mechanical Engineering Professor.
UNL College Distinguished Teaching Award (College of Engineering, spring 2011).
UNL College of Engineering College Faculty Research and Creative Activity Award, 4/10.
Dr. Megahban
M. Negahban: US Director, Advanced Mechanics and Materials Engineering International Laboratory (AMME-International), 2010

Graduate Students

NAME	PERCENT SUPPORTED
S.G.M. Hossain	
Matthew Nienaber	
Ishwari Poudel	
Eyitejumade Sogbesan	
B. J. Polly	
Sailesh Ganpule	
Aravind Sundaramoorthy	
Nikalas Lingestein	
Hao Huang	
Shawn Meagher	
Jonathan Hein	
Charles Landais	
Thomas Boulet	
Yenan Wang	
Lili Zhang	
Ashwani Goel	
J. Liu	
A. Garcia	
FTE Equivalent:	
Total Number:	**18**

Names of Post Doctorates

NAME	PERCENT SUPPORTED
Dr. Jeong Soon Lee	
Guoxin Cao	
Mehdi Sotoudeh	
Michael Arnoult	
Youn Doh Ha	
P. A. Yuya	
FTE Equivalent:	
Total Number:	**6**

Names of Faculty Supported

NAME	PERCENT SUPPORTED	National Academy Member
Namas Chandra		No
Florin Bobaru		No
Ruqiang Feng		No
Mehrdad Negahban		No
Carl A Nelson		No
Joseph A. Turner		No
Jung Yul Lim		No
FTE Equivalent:		
Total Number:	**7**	

Names of Under Graduate students supported

NAME	PERCENT SUPPORTED
Will Resse	
Brian McMichen	
John Davidson	
N. P. Waszak	
J. Dalton	
FTE Equivalent:	
Total Number:	**5**

Student Metrics

This section only applies to graduating undergraduates supported by this agreement in this reporting period

The number of undergraduates funded by this agreement who graduated during this period:	5.00
The number of undergraduates funded by this agreement who graduated during this period with a degree in science, mathematics, engineering, or technology fields:.....	5.00
The number of undergraduates funded by your agreement who graduated during this period and will continue to pursue a graduate or Ph.D. degree in science, mathematics, engineering, or technology fields:.....	3.00
Number of graduating undergraduates who achieved a 3.5 GPA to 4.0 (4.0 max scale):	3.00
Number of graduating undergraduates funded by a DoD funded Center of Excellence grant for Education, Research and Engineering:	3.00
The number of undergraduates funded by your agreement who graduated during this period and intend to work for the Department of Defense	0.00
The number of undergraduates funded by your agreement who graduated during this period and will receive scholarships or fellowships for further studies in science, mathematics, engineering or technology fields:	3.00

Names of Personnel receiving masters degrees

NAME
S.G.M. Hossain
Eyitejumade Sogbesan
Nikalas Lingestein
Shawn Meagher
Benjamin J. Polly
Total Number: 5

Names of personnel receiving PHDs

NAME
Total Number:

Names of other research staff

NAME	PERCENT_SUPPORTED
Bob Cogdill	No
FTE Equivalent:	
Total Number: 1	

Sub Contractors (DD882)

1 a. Lawrence Livermore National Laboratory

1 b. 7000 East Ave., Livermore, CA 94550-9
P.O. Box 808, Livermore, CA 94551-08

Livermore CA 94550

Sub Contractor Numbers (c): (925) 422-1100, (925) 422-4599

Patent Clause Number (d-1):

Patent Date (d-2):

Work Description (e):

Sub Contract Award Date (f-1): 10/1/2008 12:00:00AM

Sub Contract Est Completion Date(f-2): 9/30/2010 12:00:00AM

---

1 a. Sandia National Laboratories - (SNL-Livermore)

1 b. PO Box 969

Livermore CA 94550

Sub Contractor Numbers (c):

Patent Clause Number (d-1):

Patent Date (d-2):

Work Description (e):

Sub Contract Award Date (f-1): 1/10/2008 12:00:00AM

Sub Contract Est Completion Date(f-2): 9/30/2010 12:00:00AM

---

1 a. Sandia National Laboratories - (SNL-Livermore)

1 b. Combustion Research Facility
MS 9052

Livermore CA 945510969

Sub Contractor Numbers (c):

Patent Clause Number (d-1):

Patent Date (d-2):

Work Description (e):

Sub Contract Award Date (f-1): 1/10/2008 12:00:00AM

Sub Contract Est Completion Date(f-2): 9/30/2010 12:00:00AM

Inventions (DD882)

Scientific Progress

Significant theoretical or experimental advances of the RED Head (Realistic Explosive Dummy Head) Development include: Two iterations of a biofidelic headform (RED Head) have been developed with high-speed instrumentation to measure pressure, strain, etc. Shock-tube tests have been performed and data collected and analyzed. Ongoing work includes further characterization of the effects of material and geometry on shock wave propagation through these types of shock targets, including additional experimental testing.components, may further affect neuronal cell function and activity.
3.Two iterations of a biofidelic headform (RED Head) have been developed with high-speed instrumentation to measure pressure, strain, etc. Shock-tube tests have been performed and data collected and analyzed. Ongoing work includes further characterization of the effects of material and geometry on shock wave propagation through these types of shock targets, including additional experimental testing.

To read about significant theoretical or experimental advances of The Effects of Impulsive Pressurization on Brain Cell Functions see attached file.

Technology Transfer

Final Report

Army-UNL Center for Trauma Mechanics

ARO Grant W911NF-08-1-0483

(10/01/2008 -09/30/2010)

The University of Nebraska-Lincoln

College of Engineering

Lincoln, NE 68588-0642

And

U.S. Army Research Laboratory

Weapons and Materials Research Directorate

Aberdeen Proving Ground, MD 21005

March 7, 2011

Points of Contact:

Dr. Namas Chandra
College of Engineering & Technology
University of Nebraska-Lincoln
Lincoln, NE 68588-0642
Phone: (402) 472-7071
Fax: (402) 554-3850
E-mail: nchandra2@unl.edu

Ralph A. Anthenien Jr, PhD, PE
Mechanical Sciences Division
U.S. Army Research Office
Research Triangle Park, NC 27709-2211
Phone: (919) 549-4317
Fax: (919) 549-4354
E-mail: ralph.anthenien1@us.army.mil

Table of Contents

Executive Summary

The Army Research Laboratory-Weapons and Materials Research Directorate (ARL-WMRD) established a Cooperative Agreement with the University of Nebraska-Lincoln (UNL) to create a Center for Research on Trauma Mechanics and Blast Mitigation. Research conducted under this Agreement was a collaborative effort, with the ARL-WMRD and UNL sharing both leadership and research responsibilities. Research within the Center was focused on development of new materials and technologies relevant to trauma mechanics, blast mitigation and weapons detection. Specific studies within the Center were collaborative in nature, with scientific personnel from ARL interacting closely with faculty at UNL.

This report summarizes the final results achieved for specific projects performed under the Agreement. These projects had the common objective of providing new materials and technologies in the areas of trauma mechanics. The overall goal of these projects was to understand how blast waves affect the head and brain of a fully equipped soldier in the field by studying deformation and damage. This research also pursed to couple macroscopic effects with changes at the microscopic level in cells, tissues, and organs.

To achieve results UNL conducted a synergistic combination of experiments, modeling, and simulation which are unique approaches. The focus of the project was on wave propagation effects on the skull and brain especially under mild TBI pressure loading conditions. The specific objectives included:

1. Develop a state-of-the-art laboratory facility for generating well controlled air shockwaves that can mimic blast waves induced by free-field explosions and for conducting well defined and accurately measured blast wave experiments.
2. Study the effect of blast waves or pressure pulses generated on a human head with and without a protective helmet (experiments and simulation).

3. Develop a multiscale constitutive model of skull bone based on experiments and modeling. Simulate the effect of pressure and impact loading on deformation and intercranial pressure.
4. Investigate the functional and mechanical responses of neuronal cells to impulsive pressure and strain.

This research study was a combination of experiments and modeling focused on the biomechanical response of soft tissue. The experiments were designed to provide information for the modeling efforts at a variety of length scales and loading configurations such that robust, comprehensive models can be developed.

The results of these experiments were integrated with a multiscale numerical model developed at UNL and Sandia Laboratories. This model simulates blast waves at various distances and computes the pressure pulses experienced by the skull, brain, and body extremities.

Projects Conducted

This research program was comprised of 7 collaborative research projects. In this section, each of the projects is addressed individually with an overall description of the project: objective, approach, significance, and major accomplishments.

A. Laboratory Facility for Blast Wave Simulation and Experiments (Dr. R. Feng)

I. Research Objectives

The goal of this project is to develop a blast testing facility that can reliably generate air shockwaves with wave profiles mimicking those of explosion-induced blast waves in the mid- to far-field range, that ensures the test sample (head form or animal model) to be subjected to well controlled, accurately monitored, one-dimensional (1D) blast loading, and that produces time-resolved measurements of the test sample motion, deformation and pressure histories under the blast loading.

II. Approach

An explosion-induced blast wave in open field has a supersonic shock front followed immediately by blast wind with time-dependent pressure profile decaying from peak overpressure to peak underpressure (vacuum) and then recovering back to ambient. Such a wave profile is commonly described as the Friedlander wave profile. Shock tubes have been used since early 50s to generate 1D air shockwaves. In this project, the shock tube technique was adopted and specialized to generate Friedlander type of air shockwaves. We used pressurized nitrogen or helium as the driver gas and diaphragms of various designs to separate the driver section and the driven section containing ambient air. The burst pressure of each type of diaphragm was predetermined experimentally. The sudden burst of a diaphragm at its designed burst pressure allowed a rapid expansion of the driver gas into the driven section thus initiating a plane air shockwave propagating along the shock tube. Unique designs of square tube and adjustable end reflector were developed and implemented to enable the use of

high-speed digital cameras for measurement and imaging and to ensure the desired (Friedlander) wave loading. For diagnostics and control, the pressure profiles of the shockwaves at various locations along the shock tube were measured in time-resolved manner with dynamic pressure sensors.

III. Significance

The blast testing facility is a critical need for blast-induced traumatic brain injury (bTBI) research in that it enables experimental studies of the physics and mechanics underlying the transformation of blast wave incidence to brain strain and pressure, measurements of the dynamic response of skull and brain tissues and brain cells under blast loading condition, animal model experiments to determine the blast intensity thresholds and pathological mechanisms for bTBI in animal samples, and experimental evaluations of the performances of head protection systems and designs in the laboratory environment.

IV. Accomplishments

In this period, we designed and constructed two shock tubes: a 4" cylindrical uniform shock tube with variable driver and driven section lengths for pulse shaping [Fig. 1(a)] and a 9" square shock tube with optical windows for digital imaging [Fig. 1(b)]. A 28-inch square shock tube with variable driver and driven section lengths and test section position for wave profile control was also designed. A data acquisition system for up to 24 channels of synchronized time-resolved measurements at 2.5 MHz frequency and the computer program for its remote control were developed. It allows pressure profile measurements at multiple locations to accurately track the evolution of blast wave profile. A gas handling system for driver pressurization and breech firing and the network and computer program for its remote monitoring and control was developed. Capability for generating well controlled highly repeatable, shockwaves with the Friedlander wave profile was established for both the 4" and 9" shock tubes.

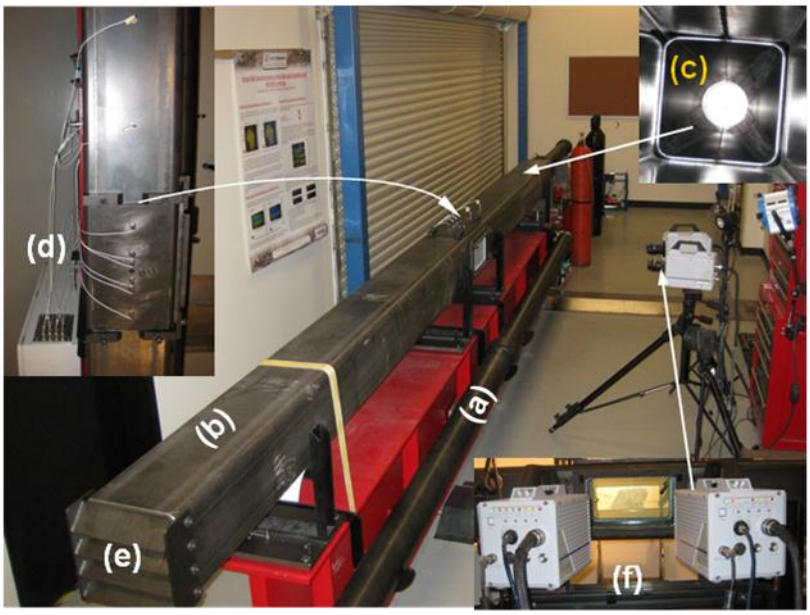

Fig. 1: Blast wave simulation and testing facility. (a) 4" cylindrical shock tube; (a) 9" square shock tube; (c) 9" tube transition section; (d) Pressure sensor array; (e) 9" tube adjustable end reflector; and (f) ARAMIS three-dimensional digital imaging system.

It was found from the results of the Experiments with the 4" cylindrical uniform shock tube that the independently measured blast wave front speed and peak pressure correlate very well with 1D shock wave theory for ideal gas giving proof that the simulated blast wave is a 1D plane wave. The device can be used for sensor calibration.

The unique 9" square shock tube has a conical transition section expanding the cross section area from that of a 4" cylindrical breech to that of a 9" square tube [Fig. 1(c)]. Although the air flow in and near the transition section is complex and multi-dimensional, it was validated experimentally that the resulting shockwave in the test section (8 ft away from the transition section) is essentially a 1D blast wave in the middle. By incorporating an adjustable end reflector at the shock tube exit, we found from experimental measurements that the amplitude and duration of the underpressure part of simulated blast wave can be well controlled with a right combination of the breech length and the end reflector position. A comparison of the pressure wave profiles with and without

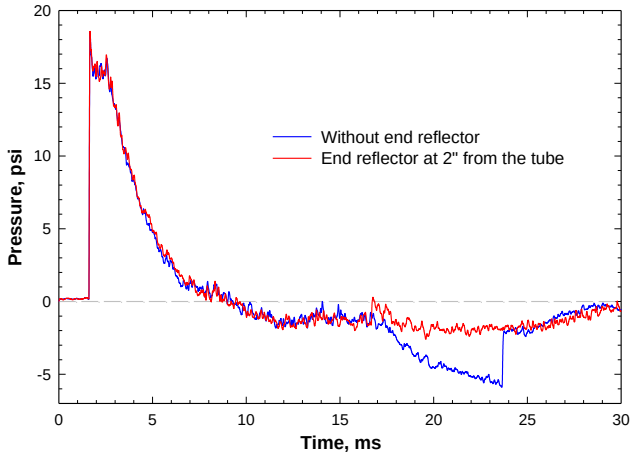

Fig. 2: Comparison of pressure wave profiles with and without adjustable end reflector.

the adjustable end reflector is shown in Fig. 2. We also successfully incorporated a state-of-the-art ARAMIS high-speed three-dimensional (3D) digital imaging correlation system into the blast testing with the 9-inch shock tube [Fig. 1(f)]. The synchronized digital imaging and 3D imaging correlation technique can provide visualization of the test sample motion under the blast loading and more importantly time-resolved measurements of the sample displacement and surface strain evolutions and therefore add a unique capability to our blast simulation and test facility.

With the 9" shock tube, we carried out a series of blast tests on tubular cylindrical polycarbonate samples of various sizes and with various fills (water, mineral oil and silicone gel). In these experiments, we used a high-precision piezoelectric sensor array to monitor the blast wave profile before and after the interaction with the test sample, the ARAMIS 3D digital imaging correlation system to measure the sample displacement and surface strain histories under the blast loading, and FISO fiber optics sensor to measure the resulting pressure history in the material filled the sample. Presented in Fig. 3 are the experimental set-up and a set of ARAMIS measurements.

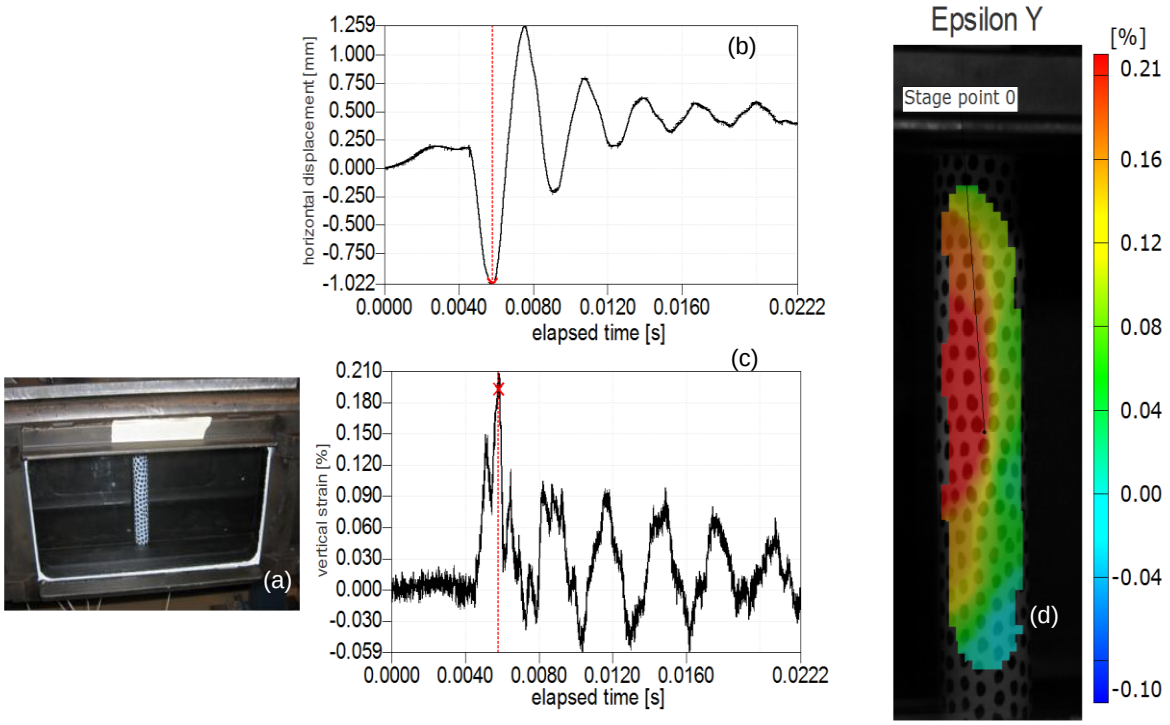

Fig. 3: Blast wave experiment on fluid-filled polycarbonate tube. (a) Experimental set-up; (b) displacement history at point 0 (near of tube side surface center); (c) Vertical strain history at point 0; (d) Snap shot of vertical strain field at the time marked with red line in

B. Realistic Explosive Dummy (RED) Head Development (Dr. Nelson)

I. Research Objectives

The main objective of this project is to create a surrogate headform whose mechanical behavior is similar to that of the human head. Through shock-tube testing of the headform and cross-validation using computational simulations, we can learn more about the possible mechanisms of blast-induced traumatic brain injury and the high-speed interactions that occur inside the head during such an event.

II. Approach

Most existing headforms are designed to replicate the amount and distribution of mass in the head but not to replicate the actual mechanical behavior of tissues in the head.

More advanced headforms may give special attention to specific structures, such as the eyes, and include some force or pressure sensors. However, no headform had previously included any truly brain-like structure or means of measuring high-speed pressure changes inside the skull cavity. Through study of the mechanical properties of the various tissue components in the human head, we were able to create a headform with mechanical behavior duplicating to a significant degree that of the human head, including the brain. We also implemented a high-speed data capture system with various types of sensors on/in the headform in order to record the phenomena occurring during shock or blast events.

III. Significance

The main significant contribution of this work is the ability to study the high-speed phenomena in the human head which may contribute to the development of traumatic brain injury in individuals exposed to blasts. This has

direct relevance to warfighter protection, care, diagnosis, and so forth. It also has similar civilian applications for industrial accidents.

By gaining a more in-depth knowledge about these phenomena, one important potential direction is development of improved protective equipment.

IV. Accomplishments

Two iterations of a biofidelic headform (RED Head) have been developed with high-speed instrumentation to measure pressure, strain, etc. Shock-tube tests have been performed and data collected and analyzed. Ongoing work includes further characterization of the effects of material and geometry on shock wave propagation through these types of shock targets, including additional experimental testing.

C. TBI-Materials Modeling and Characterization and 3-D Optical Measurements (Dr. Negahban)

I. Research Objectives

1) Modeling and Characterization

The materials modeling and characterization group has been working on characterizing the skin, skull and brain, and the associated natural and man-made materials used in the design and construction of the RED-Head, in protective components, and the blast facility. The experimental setup and numerical analysis within the TBI blast community and the UNL Blast facility need accurate material properties and models for the different components that compose the human and animal testing setups, the dummy RED-Head, and protective armor. The group works to collect data, develop new experimental techniques, and construct models to better support the communities ability simulate, design, and develop systems to protect against TBI.

2) 3-D Optical Measurements

The 3-D optical measurement group works with provide continuous surface strain measurements capabilities and develop this technique for dynamic testing system. In doing so the group supports the RED-Head group, the dynamic testing group.

II. Approach

Since the modeling and characterization group worked to support many different constituents, the approach taken included:

(a) In support of the RED-Head development and materials characterization we conducted dynamic mechanical testing (DMA) on materials being considered and used in the RED-Head. This included DAM results in compression, double shear, and/or cantilevered beam modes for the polymer skin and skull materials provided by the manufacturer of the RED-Head and for

different silicone gels and other materials considered for the brain. Similar tests were conducted on pig brain, liver, and cow hip bone to provide a comparative measure between the artificial materials used in the RED-Head and biological materials (Fig. 4); (b) In an effort to consider how to improve the skull model to better mimic the actual skull, we did an experimental study of the effects of different microstructures on the average ultrasonic signal transmitted through polymer samples with different patterns of voids constructed using rapid prototyping; (c) In an effort to better characterize the bone structure in the skull, we conducted a study of the anisotropic properties of bovine hip bone taken along different directions using both DMA and ultrasonic waves; (d) In an effort to overcome the strong dissipation that controls the possibility of measurements in soft tissue, and in particular the brain, we have been developing a method to characterize the wave speed and attenuation under load using reflected signal changes at different frequencies; (e) To improve models currently used in the simulation of the skin, skull and brain, we constructed viscoelastic models to characterize both the shear and dilatational response of these components under infinitesimal deformations using Prony series models of the relaxation; (f) To better capture the dynamic response of the brain we developed a method to fit a continuous relaxation function to shear data, allowing a much better fit of both the storage and loss moduli; (g) To capture the nonlinear response of the skin, skull and brain under the more realistic nonlinear setting, we have been developing a theory for wave propagation in nonlinear viscoelastic materials.

Since the 3-D optical measurement group work in both development of technique and support of current activities by other groups working on the TBI project, the work took different approaches to the different responsibilities that included working with the RED-Head group, the dynamic testing group, and the blast facility to conduct low and high speed optical measurements in support of the following activities: (a) Support of the RED-Head in conducting dynamic testing on different gels for use as the brain simulation material; (b) Dynamic characterization of the blast facility, including the characterization of the effect of

windows, characterizing the shock induced change in the index of diffraction of the gas, and general high speed measurements during development of the facility; (c) Dynamic characterization of sample surface deformation inside and outside the blast tube for both the RED-Head and simple sample geometries used to calibrate the gun, the measurement systems and the computer simulations; (d) High speed characterization on the Kolsky bar and on other setups (Figs. 5 and 6).

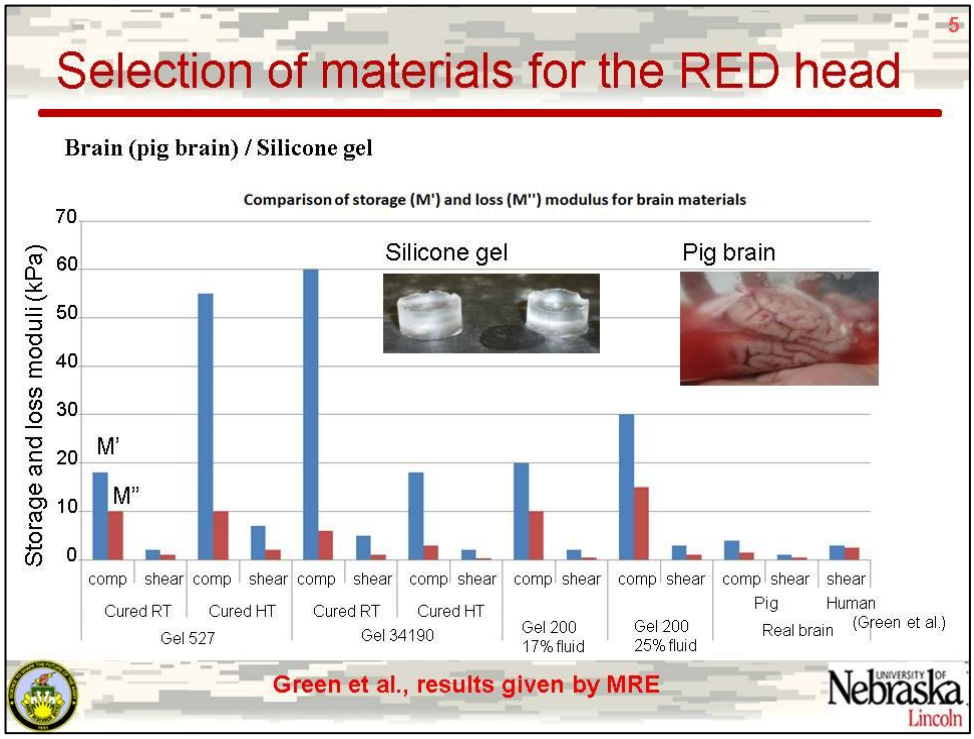

Fig.4: Comparing model materials and true response.

III. Significance

The constitutive characterization and modeling group both established support the design, development, and analysis TBI facility and worked on the development of new characterization methods for soft tissues and large deformations.

The 3-D optical measurement group developed optical characterization competencies for quasi-static to dynamic surface strain measurements using an ARAMIS low and high speed system, and supported the design and the development of the blast facility.

Fig. 5: 3-D Optical measurement for characterization of blast wave distortion.

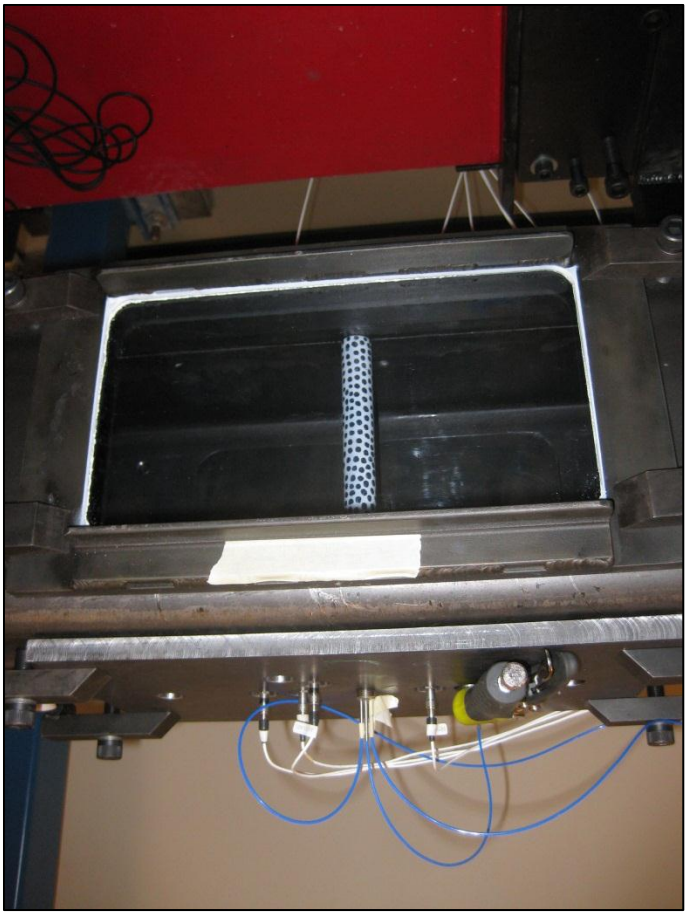

Fig. 6: 3-D Optical measurement for characterization of blast interaction with a cylinder.

IV. Accomplishments

(1) The group established mechanical characterization between human and animal head components including skin, bone, and brain, and their counterparts used in the RED-Head.

(2) The group established improved modeling for the characterization of skin, skull, and brain viscoelastic properties.

(3) The group improved the modeling of the linear viscoelastic modeling of head components by developing a continuous response spectrum (Fig. 7).

(4) The group worked on characterization techniques for obtaining elastic and viscoelastic properties of highly attenuating materials such as biological tissue using wave reflection methods and conducted preliminary evaluations.

(5) The group worked on perturbation in nonlinear viscoelastic loaded materials to establish a better characterization/modeling method for biological materials undergoing large deformations.

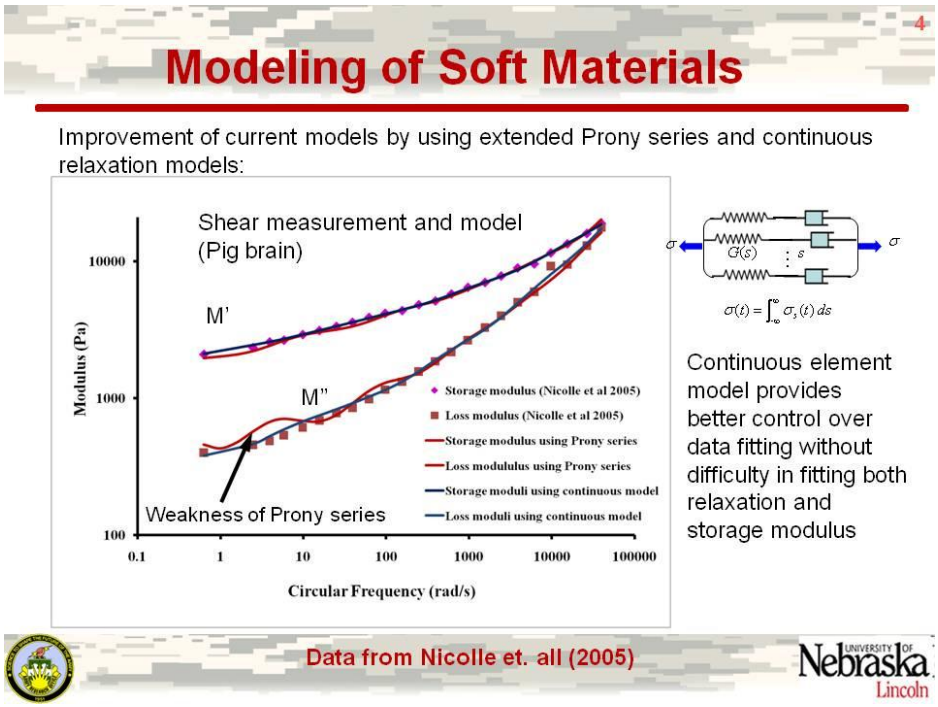

Fig. 7: Improving modeling by using continuous spectra.

D. Influence of Skull Microstructure on the Profile of Pressure Waves (Dr. Turner)

I. Research Objectives

The objective of this project is to quantify the influence of skull microstructure on the profile of pressure waves that pass through the skull.

II. Significance

The flat bones of the skull are comprised of the outer and inner tables (compact bone) and the diploe (porous bone) on the interior. This variation in microstructure within the skull causes a disruption in the coherent nature of waves that are incident on the skull. Blasts that result from IEDs and other small ordnances are often characterized by a fast rise time such that they are fairly broad band (up to ~1 MHz in frequency content).

The scattering behavior that will result from the skull microstructure will reduce the pressure profile (i.e., strain) and alter the frequency content (i.e., strain rate) of the incident wave. Currently, very little is known about the cells of the brain with respect to their response to excitations that include a wide frequency range since strain rate effects on single cells or groups of cells remains largely unexplored. Thus, a clear understanding of the influence of skull microstructure on wave transmission is needed. As part of the proposed research, a variety of techniques will be used to quantify this behavior and connect the skull architecture to the wave behavior. Human skull samples will be used as the basis for all measurements so that the results will be directly applicable to the warfighter.

III. Accomplishments

Previous research on this aspect of the TBI research was started in the last two years at UNL in the PI's group. A human skull sample was obtained from UNMC in order to begin exploration of this research area that has been largely

neglected. The sample was obtained from a healthy 78-year-old male patient who required brain surgery (Fig. 8).

The skull piece could no longer be replaced after the surgery and was provided for this research. Small samples were cut from the larger sample so that microstructure and property information could be obtained. MicroCT and nanoindentation measurements were made on the four samples to quantify these aspects of the skull response. Porosity ranged from 17-30 % and the storage modulus was in the range of 20 GPa. The optical images were used to construct 2D finite element (FE) models so that an initial understanding of the influence of microstructure could be obtained.

The FE models were developed using ABAQUS software and are highlighted in Fig. 2. The model consisted of a region that represented the skull (either as solid or porous) and a region that represented the brain (modeled as a fluid). Different pressure profiles, exciting the entire top surface of the model, were explored as incident wave inputs including a three-cycle Gaussian pulse and a profile representative of a blast pulse.

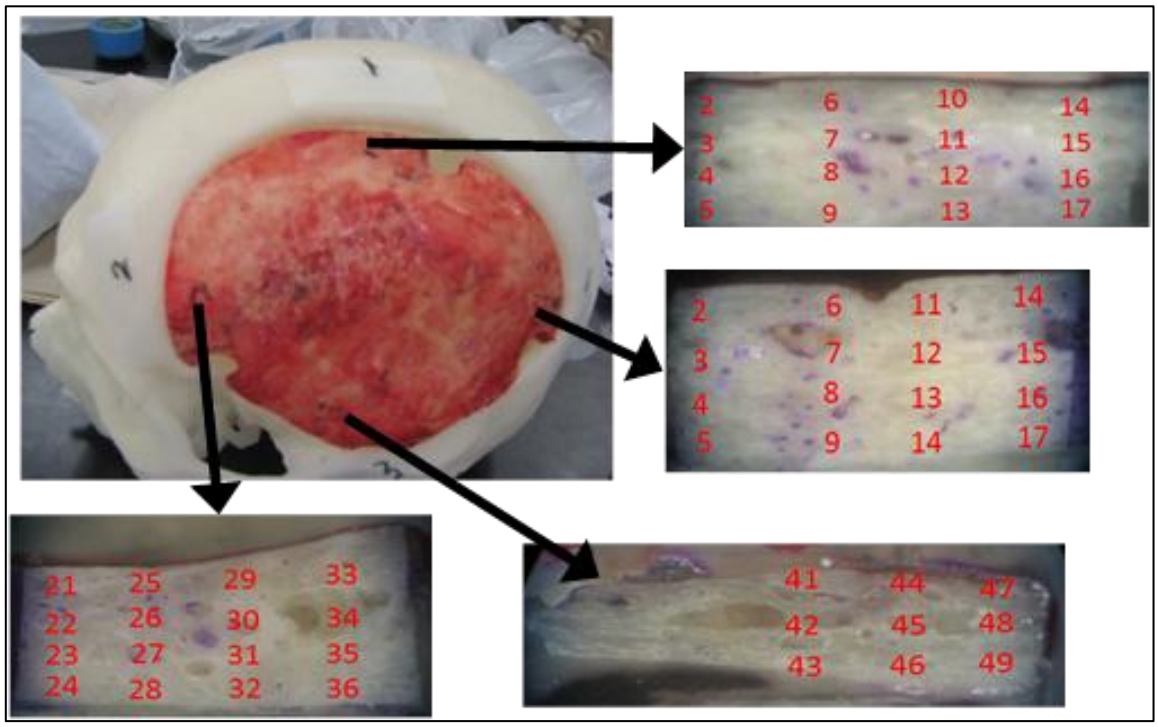

Fig. 8: Example skull sample obtained from UNMC (Dr. P. Lennarson). Four samples were cut from the larger sample. The smaller samples were used to get microstructure information (using microCT) and viscoelastic property information (using nanoindentation).

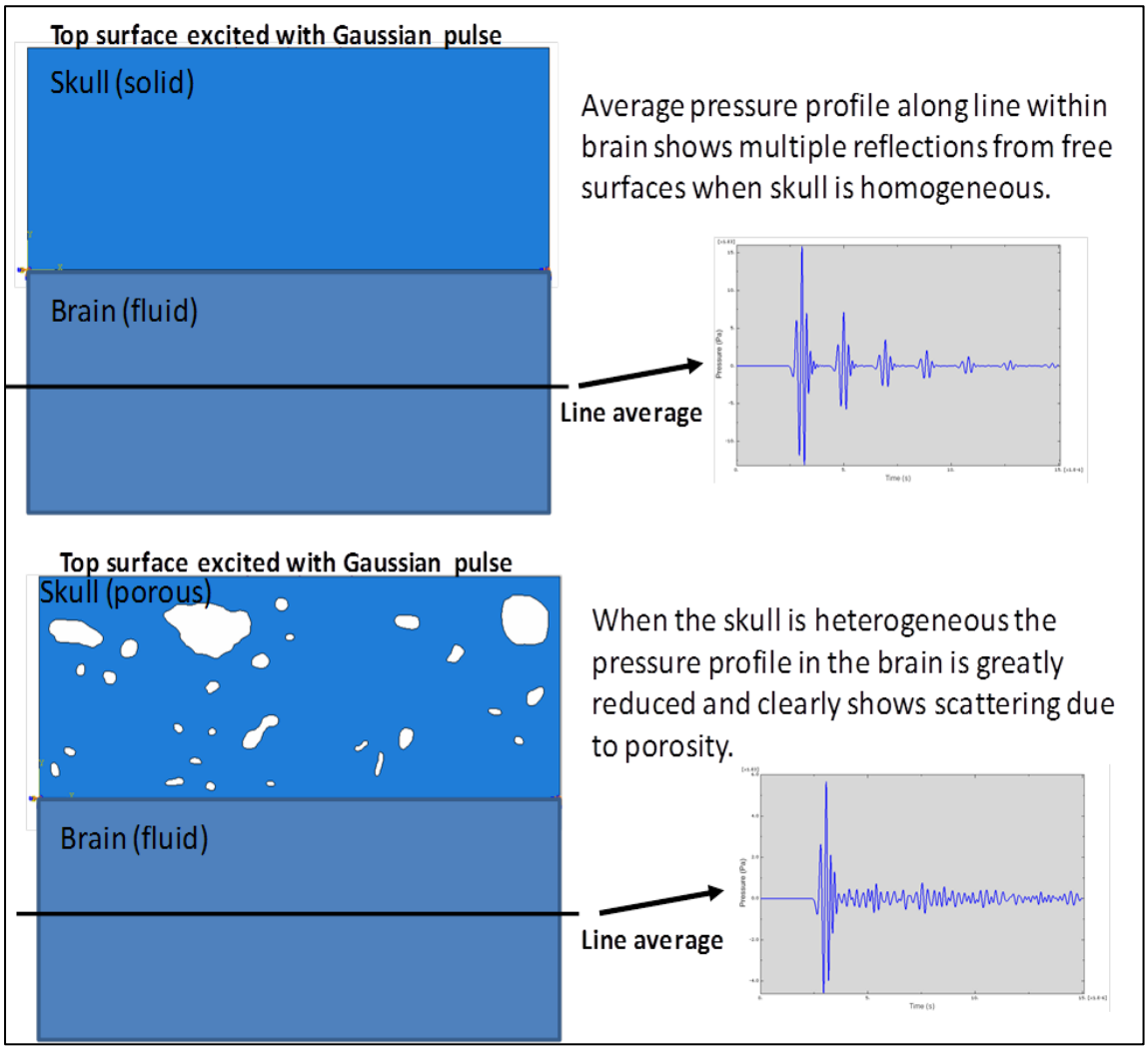

Fig. 9: Example finite element results that highlight the potential impact skull microstructure can have on the transmission of pressure through the skull.

E. Fluid-Structure Interaction (FSI) (Dr. Bobaru)

I. Research Objective

Many of Traumatic Brain Injury (TBI) phenomena involve complex Fluid-Structure Interaction (FSI) induced by blast waves propagation. The objective of this part of the project was to find and develop numerical verification methods for the simulation of the FSI problem to better understand the mechanical behavior of a three-dimensional test sample in a shock tube experimental setup. The goal was to model, at the same scale and geometry as the shock tube developed and used in experiments performed by another group (Dr. Feng) on the same project. The computational model we provided helped the experimental group to design more reliable experiments and improve the actual shock tube. For example, better location of the sensors on the sample tested was found using our computational models.

II. Approach

The main target model was the UNL Shock Tube facility (Dr. Feng group). We modeled the propagation of blast waves using the same geometry and scale as the actual shock tube and using the same blast wave generation mechanism that induced the blast wave in experiments. We first verified the main characteristics of blast wave propagations, such as the shape of blast wave profile, peak pressure magnitude, etc. We employed the finite volume method built in ABAQUS. We constructed the model for the blast wave generation mechanism and implemented this into ABAQUS. Next, we modeled the coupled FSI problem by coupling the immersed finite element method (for the solid materials) with the finite volume method (for the fluid part). Many challenging issues around the intermediate region shared by both solid and fluid elements arose: inconsistent boundary, contact condition, etc. We found solutions to these issues. We investigated the correlations of the fluid pressure magnitude and profile ahead and around the solid obstacle and compared with experiments.

III. Significance

Understanding the fluid-structure interaction in blast conditions is paramount to progress in the TBI problems. The design of experiments in the shock tube used the results we produced for their calibration and testing.

IV. Accomplishments

In this small-scale portion of the project we have developed the generalized Fluid-Structure Interaction (FSI) computational model in ABAQUS and performed computations for the experiments conducted by Dr. Feng's group at UNL's shock tube facility.

F. Effects of Impulsive Pressurization on Brain Cell Functions (Dr. Lim, Dr. Feng)

I. Research Objectives

A blast-induced traumatic brain injury (bTBI) caused by exposure to blast of various explosive devices, including improvised explosive device (IED), may result in post-concussion symptoms that are easily overlooked immediately after the event but pose long term health problems. A better understanding of the cellular level mechanisms, through which an IED blast induces the primary bTBI and its secondary progression, is critically important for developing effective protection gears, early diagnostics techniques/procedures, and proper treatments against bTBI.

II. Approach

To investigate the role of dynamic short-duration overpressure (one of the speculated factors) in the brain cell response to bTBI relevant blast loading, we have developed novel impulsive brain cell pressurization equipment based on Kolsky bar set-up. This apparatus allows examination of brain cell functions after exposure to in vitro conditions mimicking blast-induced pressure loading.

III. Significance

Currently, bTBI is measured using a combination of magnetic resonance imaging (MRI) and the assessment of the duration of loss of consciousness or amnesia. However, no technology currently exists for reliably replicating the blast loading of the brain cells in vitro. While the mechanism of how blast waves affect the brain and brain cells is not fully revealed, collective data suggest that bTBI is a short-duration overpressure-induced, stress wave-dominant phenomenon. Therefore, the development of technology that enables the evaluation of impulsive overpressure effects on brain cells, in both short and long-term perspectives, under bTBI relevant blast loading conditions will provide a huge opportunity to reveal the nature of bTBI.

IV. Accomplishments

A technique to generate fast-rising, long-duration, single compressive stress pulses has been developed by incorporating a new axial loading system (which consists of a two-way hydraulic piston and an inertia stopper) in a Kolsky torsion bar device available in Feng's lab (Laboratory for Dynamic Materials Characterization). A cell pressurization chamber that can convert axial stress pulse imposed on its exterior to well defined pressure pulse in the culture medium fluid contained in its interior has been developed. The fixation of cell cultured glass slide within the chamber has been accomplished. The top view of Fig. 10 shows the Kolsky bar cell pressurization set-up and schematic of force transfer during the pressurization. Using this apparatus, single compressive stress pulses with a rise time of approximately 0.05 ms, a pulse duration of approximately 0.7 ms, and stress levels at 0.5-2 MPa have been accomplished as a transient overpressure stimuli to the cultured neuronal cells. The bottom view of Fig. 10 shows an example that 0.5, 1, and 2 MPa level impulsive pressurizations.

Human SH-SY5Y human neuroblastoma cell (ATCC, CRL-2266) culture and pressurization protocols have been established. Before pressurization, SH-SY5Y cells were treated with 10 μM retinoic acid (RA) for 7 days for neurite/axonal outgrowth. Cells treated with RA the same, placed inside the pressurization vessel the same, but not pressurized served as an unpressurized chamber control. Effects of bTBI relevant impulsive pressurization on the cytoskeletal structure of neuronal cells were examined (Fig. 11). Two of the important cytoskeletal structures, actin (red) and tubulin (green), were clearly observed in the unpressurized control cells following the neurite/axonal structure. Neuronal cells exposed to impulsive pressurization at 2 MPa magnitudes and 0.7 ms duration showed distinct breakdown of the neurite/axonal structure, as seen by shorter or no actin/microtubule staining. Microtubules serve not only as cytoskeletal components but also play a role as a marker of neurogenesis. Microtubles are heavily involved in the expression of microtubule-associated

protein-2 (MAP2), which is a distinct marker of neuronal differentiation. Our data thus suggest that bTBI-relevant pressurization, that induces changes in apparent neurite morphology and cytoskeletal components, may further affect neuronal cell function and activity.

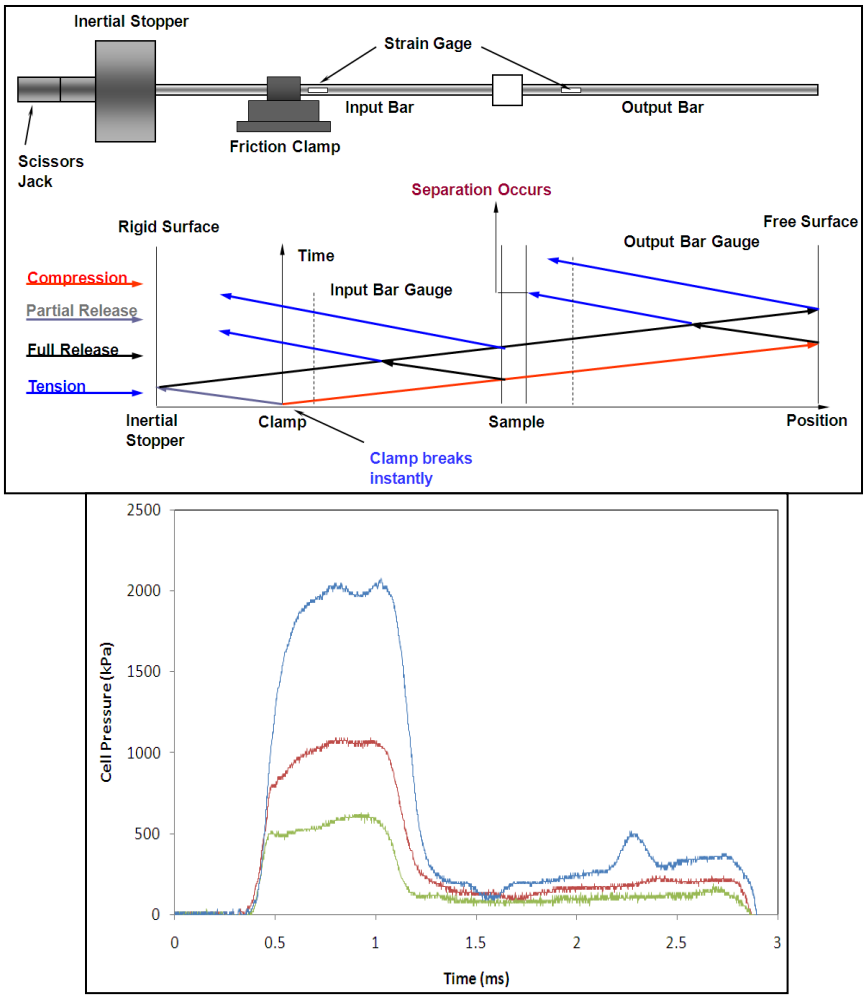

Fig. 10: Schematic of impulsive cell pressurization device based on Kolsky bar. The bottom diagram shows schematic of force transfer during the pressurization.

We could control the impulsive pressurization levels at 0.5-2 MPa magnitude. The pressures recorded with a Fiso pressure gauge had the same square pulse shape as the transmitted bar measurements.

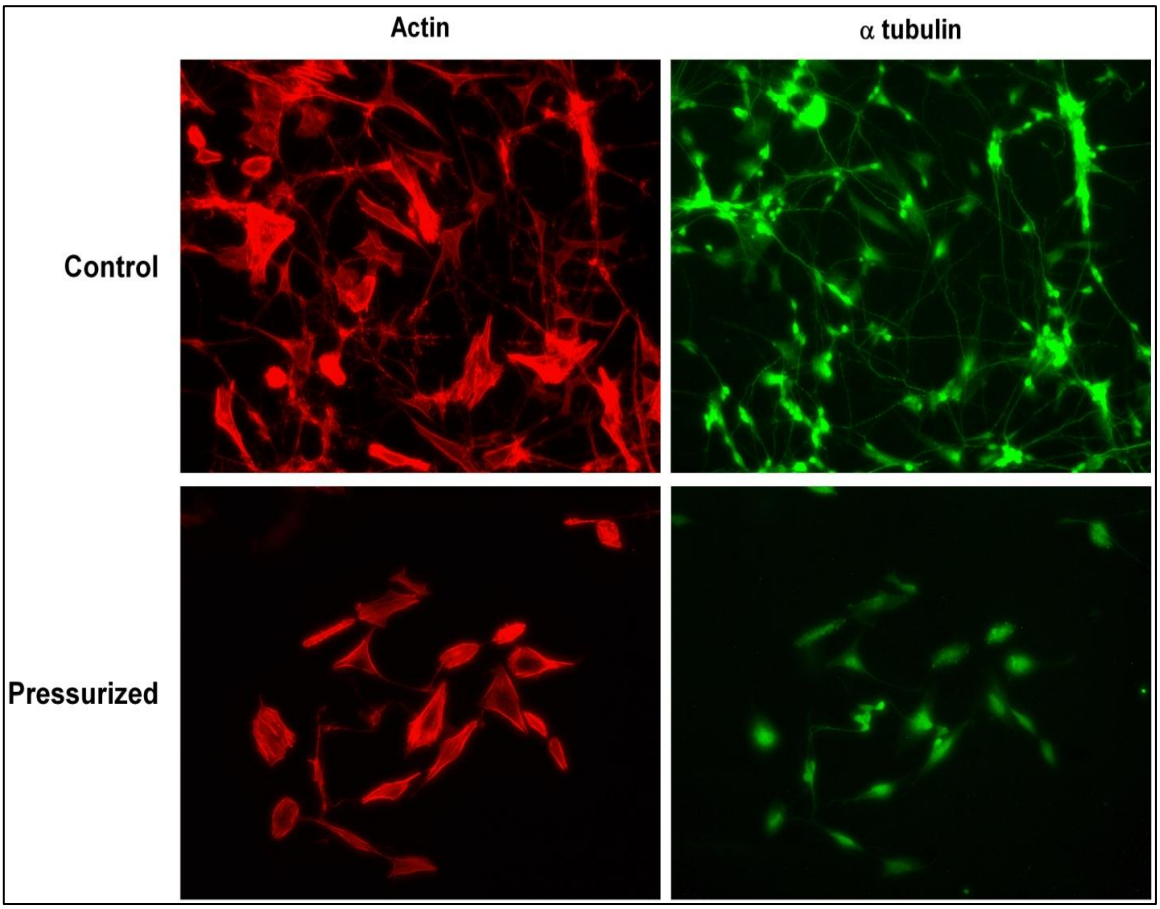

Fig. 11: Human neuronal cells pressurized at 2 MPa and 0.7 ms duration display distinct neurite/axonal breakdown relative to chamber control cells, e.g., shortened or removed neurite/axons in the immunofluorescence of actin (red) and α tubulin (green).

G. Computational Modeling of Human Head and Testing of Neurons (Dr. Chandra)

I. Research Objectives

1) Modeling, simulation of the head (brain) of war fighters (humans) with high biofidelic anatomical details.
2) Examine the role of protective helmets in mitigating the effect of shock-blast induced by IEDs.
3) Mechanisms of deformation and damage of in-vitro neurons and high rates of loading.

II. Approach

Modeling and simulations: Integrate a series of medical MRI and CT images and construct a 3D brain-head model. The model is anatomically accurate; and can be discretized into finite elements for analysis and validation with experimental results.

Role of protective helmets: Digitize accurately helmets of various generations and origin and import into numerical models. Include the effects of harness and various pads with high geometric accuracy. The effect of helmets can be analyzed by understanding the mechanics of shock-blast interactions with the head.

In-vitro neuron testing: Culture human neurons in the laboratory and test them under different strain-rate and establish strain-response curves. The response may be biochemical alterations of proteins or necrosis.

III. Significance

Blast TBI is one of the critical unresolved issues that have a political, economic and personnel consequences to US army. Understanding if and why blasts cause mild TBI is very timely. Once mechanisms are identified then mitigative strategies can be formulated.

IV. Accomplishments

Significant progress has been made in the modeling aspects. We now can build accurate geometric and biofidelic models and simulate shock-blast interactions.

Technology Transfer

I. The 'RED Head' or 'Realistic Explosive Dummy Head' development project focuses on head injuries caused by shock waves generated by explosions. To develop such a head model, materials analysis was performed to find synthetic materials to simulate human head components such as skin, skull and brain. The geometries of these components were carefully controlled to simulate it as a human head surrogate. The head model was instrumented with various sensors to understand the attenuation of the pressure waves through the brain and the flexure of the skull. The prototypes developed as part of this project are available for loan to and use by DOD or other personnel if desired. The details of their design can also be shared and have been presented to some extent in publications, and presentations which have been shared in the 2009 summer progress meeting with DOD personnel.

II. The numerical models developed in ABAQUS can be used by researchers at DoD to better understand the complex behavior of structures and systems under blast conditions.

III. Throughout the funding period, constant interactions with US army (ARO, PEO, ARL, US Army Medical command) occurred. The PI Dr. Namas Chandra is a part of an expert panel organized by Michael Leggiri. He also presented his findings in the army meeting at St. Petersburg in June 2010.

Publications and Presentations (*: graduate students supported by the ARO grant)

I. Journal Articles

- G. Cao and Chandra, N. Evaluating the Biological Cell Properties Using Dynamic Indentation Method, **Physical Review E**, 81, 021924, 1-9, (2010).
- A. Goel*, M. Negahban, L. Zhang*, "Modeling nonlinear thermo-elastic response for glassy polycarbonate using ultrasonic results under compression in a confined cell," Mechanics of Materials (doi:10.1016/j.mechmat.2011.02.006).
- Matthew Nienaber,** Jeong Soon Lee,** Ruqiang Feng, Jung Yul Lim. Impulsive pressurization of neuronal cells for traumatic brain injury study. *J. Vis. Exp.* submitted (**: contributed equally).
- Matthew Nienaber, Jeong Soon Lee, Jung Yul Lim, Ruqiang Feng. Kolsky bar based cell pressurization device mimicking blast-induced traumatic brain injury conditions. *J. Biomech.* In preparation.

II. Conference Presentations

- G. Cao and N. Chandra, "Substrate Effect on Dynamic Indendation Measurement of Biological Cell Properties," Materials Research Society (MRS) Spring Conference, San Francisco, California, April 2009.
- K. Strabala*, L. Delbreilh*, J.-M. Saiter, M. Negahban "Effects of compression and aging on the fracture, mechanical, and thermal properties of glassy polycarbonate," 17thWorld Forum on Advanced Materials (PolyChar 17), Rouen, France, April 20-24, 2009.
- M. Negahban, A. Goel*, K. Strabala*, J. Vogeler*, R. Feng, "Experimental characterization and constitutive modeling of polycarbonate under change of temperature, strain and strain rate," 17th World Forum on Advanced Materials (PolyChar 17), Rouen, France, April 20-24, 2009.

- G. Shailesh, G. Cao and N. Chandra, “Computational Simulation of the Helmet Effect on the Blast Induced Traumatic Brain Injury,” 10th U.S. National Congress on Computational Mechanics, Columbus, Ohio. July, 2009.
- S. Ganpule, L.X. Gu, and Chandra N., Role of Helmet in Mitigating Traumatic Brain Injury, BMES Annual Fall Meeting: Bridging Biology, Engineering and Medicine, Pittsburgh, PA, October 7-10, 2009.
- G. Cao and N. Chandra, “Evaluating the Nucleus Effect on the Cell Mechanical Behavior,” 2009 ASME International Mechanical Engineering Congress and Exposition (IMECE09), Lake Buena Vista, Florida, November, 2009.
- G. Sailesh, L. Gu, G. Cao and N. Chandra, “Role of Helmet on Mitigating the Blast Induced Injury,” ASME International Mechanical Engineering Congress and Exposition (IMECE09), Lake Buena Vista, Florida, November 13-19, 2009.
- G. Shailesh, L. Gu, G. Cao and N. Chandra, The Effect of Shock Wave on a Human Head, 2009 ASME International Mechanical Engineering Congress and Exposition (IMECE09), Lake Buena Vista, Florida, November 13-19, 2009.
- G. Cao and N. Chandra, Evaluating the Mechanical Behavior of Biological Cell Based on Scanning Probe Indentation, the 3rd International Conference on Mechanics of Biomaterials & Tissues (ICMOBT), Clear Water Beach, Florida. December, 2009.
- L Zhang*, T. Boulet*, J. Hein*, M. Negahban, “Material Characterization and Modeling of Head for Dynamic Simulations,” International Conference on Computational & Experimental Engineering and Sciences, ICCEES’10, Las Vegas, USA, March 28-April 1, 2010.
- M. Negahban, A. Goel, L. Zhang*, K. Strabala*, Q. Fichot*, F. Souza, S. Meagher*, J. A. Turner, D. Allen, J.-M. Saiter, L. Delbreilh, “Plasticity-like modeling of nonlinear viscoelastic response and its application to glassy

polymers and biological tissue," Composites and Infrastructures Workshop, Verese, Italy, May, 2010.

- M. Negahban, A. Goel, L. Zhang*, K. Strabala*, Q. Fichot*, F. Souza, S. Meagher*, J. A. Turner, D. Allen, et L. Delbreilh, "Characterization, Modeling, and Consequences of the Development During Plastic Flow of Large Anisotropy in the Wave-Speeds and Fracture," in New Models and Hydrocodes for Shock Wave Processes, Paris, France, May 24-28, 2010
- M. Nienaber, J. G. Vogeler, and R. Feng, "A Kolsky Bar Technique for Impulsive Fluid Pressurization," 2010 SEM Annual Conference & Exposition Indianapolis, IN, June 7-10, 2010
- G. Cao, Y. Zhou, J.S. Lee, J.Y. Lim, and N. Chandra, "Mechanical Model of Neuronal Function Loss," 16th US National Congress of Theoretical and Applied Mechanics (USNCTAM2010), State College, PA, June 27-July 2, 2010.
- S. Ganpule, L.X. Gu, and N. Chandra, "Modeling Shock Response of Human Head Using Fluid-Structure Interaction (FSI)," 16th US National Congress of Theoretical and Applied Mechanics (USNCTAM2010), State College, PA, June 27-July 2, 2010.
- Namas Chandra, "Trauma Mechanics Research: Helmet design, brain and skull modeling," UNL Pentagon Research Meeting, 28 July, 2010.
- N. Chandra, "Micromechanical Injury Threshold Models of Neurons-Experiments and Theory," DOD Brain Injury Computational Modeling Expert Panel Meeting, St. Pete Beach, Florida, August 2010.
- M. Negahban, A. Goel, K. Strabala*, "The role of evolving anisotropy in modeling the small and large deformation thermodynamic viscoealstic and viscoplastic response of glassy polymers," 7th International Conference on Mechanics of Time-Dependent Materials, Portoroz, Slovenia, September 5-11, 2010.

- Youn Doh Ha, Shailesh Ganpule, Florin Bobaru, and Ruqiang Feng, "Fluid-structure interaction models of air blast on head," 47th Annual Technical Meeting of Society of Engineering Science, Iowa state university, Ames, IA, October 3-6, 2010.
- Aaron D. Holmberg, Nicholas N. Kleinschmit, Ruqiang Feng, Youn Doh Ha, and Florin Bobaru, "Shock-tube-simulated blast wave propagation and interactions with solid structures," 47th Annual Technical Meeting of Society of Engineering Science, Iowa state university, Ames, IA, October 3-6, 2010.
- S.G.M. Hossain, Mickael Arnoult, Thomas Boulet, Charles Landais, Jonathan Hein and Carl Nelson, 2010, "Material Analysis for the Development of a Surrogate Headform to be Tested Under Blast-Induced Shock Loading," 47th Annual Technical Meeting of Society of Engineering Science, Iowa state university, Ames, IA, October 3-6, 2010.
- N. N. Kleinschmit, A. D. Holmberg, and R. Feng, "Wave Profile Shaping for Shock-Tube-Simulated Blast Testing," 47th Annual Technical Meeting of Society of Engineering Science, Iowa state university, Ames, IA, October 3-6, 2010.
- S. Meagher*, K. Strabala*, C. Landais*, L. Delbreilh, M. Negahban, J. Turner, "Anomalous Loss of Toughness with Physical Aging of Work Toughened Polycarbonate," 47th Annual Technical Meeting of Society of Engineering Science, Iowa State University, Ames, IA, October 3-6, 2010.
- M. B. Nienaber, J. S. Lee, R. Feng, and J. Y. Lim, "Impulsive Pressurization of Neuronal Cells," 47th Annual Technical Meeting of Society of Engineering Science, Iowa State University, Ames, IA, October 3-6, 2010.
- X. Shi, M. Nienaber, R. Feng, and M. Negahban, "A Long-Pulse Kolsky Bar Technique for Dynamic Testing of Soft Biomaterials," 47th Annual Technical Meeting of Society of Engineering Science, Iowa State University, Ames, IA, October 3-6, 2010.

- J. Hein*, B. McMichen*, A. Stibbe*, M. Negahban, D. Cullen, J. Turner, M. Akhter, “Mapping tibial surface strains using 3D stereo optical system,” (poster) ASBMR 2010 Annual Meeting, Toronto, Canada, October 16-18, 2010.
- L. Zhang*, M. Negahban “Wave prorogations in pre-deformed nonlinear viscoelastic materials,” 47th Annual Technical Meeting of Society of Engineering Science, Iowa State University, Ames, IA, 3-6 October, 2010.
- S. Ganpule, L.X. Gu, and N. Chandra, “MRI-Based Three Dimensional Modeling of Blast Traumatic Brain Injury,” 2010 ASME International Engineering Congress and RD&D Expo, Vancouver, British Columbia, Canada November 12-18, 2010
- S. G. M. Hossain, C. A. Nelson, T. Boulet, M. Arnoult, L. Zhang, A. Holmberg, J. Hein, N. Kleinschmit, E. Sogbesan, “Material Modeling and Development of a Realistic Dummy Head for Testing Blast Induced Traumatic Brain Injury,” IV European Conference on Computational Mechanics – ECCM 2010, Paris.

Awards and Honors

Awarded to Dr. R. Feng (2008-2010)

- Fellow, American Society of Mechanical Engineers, December 2008.
- Certificate of Recognition for Contributions to Students, Parents Association and Teaching Council, University of Nebraska-Lincoln, 2008.
- Faculty Research and Creative Activity Award, College of Engineering, University of Nebraska-Lincoln, 2009.

Awarded Dr. C.A. Nelson (2008-2010)

- ME Department 2008-09 Teaching Award, University of Nebraska-Lincoln.
- Henry Y. Kleinkauf Family Distinguished New Faculty Teaching Award, College of Engineering, University of Nebraska-Lincoln, 2010.
- Outstanding Mechanical Engineering Professor, UNL Pi Tau Sigma Golden Key Award 2009-2010.
- Faculty Research and Creative Activity Award, College of Engineering, University of Nebraska-Lincoln, 2010.

Awarded to Dr. M. Negahban (2008-2010)

- US Director, Advanced Mechanics and Materials Engineering International Laboratory (AMME-International), 2010.

Students and Postdocs Supported or Partially Supported by the ARO Grant

BS:

- Brian McMichen, "Stereo optical characterization of effects of osteoporosis in mouse bone models," UNL Undergraduate Research Experience (Ucre), 2009-2010.
- John Davidson, "Characterization of failure in soft materials," Ucre, 2009-2010.
- N. P. Waszak
- J. Dalton

MS:

- S.G.M. Hossain, MS in Mechanical Engineering, August 2010 (currently pursuing PhD at UNL).
- Aaron B. Holmberg, MS in Engineering Mechanics, December 2010.
- Shawn Meagher, double MS: Engineering Mechanics, University of Nebraska-Lincoln, and Materials Engineering, University of Rouen, Rouen, France, December 2010.
- Charles Landais, double MS: Engineering Mechanics, University of Nebraska-Lincoln, and Materials Engineering, University of Rouen, Rouen, France, expected May 2011.
- Eyitejumade Sogbesan, MS in Mechanical Engineering, expected May 2011.
- Jonathan Hein, MS in Engineering Mechanics, expected May 2011.
- Nickolas N. Kleinschmit, MS in Engineering Mechanics, expected August 2011.
- Matthew B. Nienaber, MS in Engineering Mechanics, expected August 2011.
- Garcia, MS in Engineering Mechanics, expected December 2011).
- Ishwari Poudel, MS, Engineering Mechanics, in progress.

PhD:

- Ashwani Goel, PhD, Engineering Mechanics, December 2009.
- Lili Zhang, PhD, Engineering Mechanics, expected August 2011.
- Jianbin Zhu, PhD, Engineering Mechanics, expected August 2011.
- Jinjin Liu, PhD, Engineering Mechanics, in progress.

- Thomas Boulet, PhD, Biomedical Engineering, in progress
- Yenan Wang, PhD, Engineering Mechanics, in progress

Postdocs:

- Dr. Jeong Soon Lee, Post-Doctoral Research Fellow at UNL since 2009.
- Dr. Michael Arnoult, currently Research Coordinator for Upper Normandy, France.
- Dr. Y.D Ha, Post-Doctoral Research Associate, UNL.

Appendix

IMECE2010-39428 Technical Publication

MRI-Based Three Dimensional Modeling of Blast Traumatic Brain Injury (bTBI)

Authors

SHAILESH GANPULE, University of Nebraska Lincoln

Linxia Gu, University of Nebraska-Lincoln

Namas Chandra, University of Nebraska-Lincoln

Abstract

Blast induced traumatic brain injury (bTBI) is signature injury in recent combat scenarios involving improvised explosive devices (IEDs). The exact mechanisms of bTBI are still unclear and protective role of helmet and body armor is often questioned. Because of the complex and highly nonlinear fluid-structure interactions involved in bTBI and the limitation of diagnostic methods in comparison, robust computational modeling with experimental validation is necessary in order to understand mechanisms of bTBI. In an effort to understand the mechanics of blast-induced traumatic brain injury (bTBI), we have built numerical head models utilizing the arbitrary Euler-Lagrangian coupling method available in the ABAQUS finite element code. Our simulation methodology allows accurate concurrent simulations of the formation and propagation of blast-like air shockwave, the fluid-structure interactions between the shockwave and the head, and the stress wave propagation within the head. In this method, an Eulerian mesh is used to model the air surrounding the head and a Lagrangian mesh is used to model the head. The shock wave is generated by releasing high pressure, high temperature compressed air into the atmospheric air at the beginning of the analysis. The predefined pressure and temperature of compressed air is adjusted so as to generate blast overpressures equivalent to blast overpressures in nonlethal blast injury, threshold lung injury and 50% lethal lung injury. We have built two types of numerical head models. The first head model is surrogate dummy head model consisting of skin, skull, brain and the neck. The material properties for various head components such as dummy skull,

dummy skin and brain simulant are obtained from various tests performed in house. This dummy head model is validated against shock tube experiments conducted in in-house shock testing facility. This model has served as 'benchmark' for our modeling effort and suggests reliability of our modeling effort. Second head model is anatomically detailed three dimensional head model (real head model from here on) developed from segmentation of MRI images available from Visible Human Project of the National Library of Medicine . This model consists of anatomical details of head such as skull, ventricle, white matter, grey matter, CSF, air sinus, tentorial membranes and falx. The material properties of various tissues of the real head model are either taken from literature or obtained from in-house testing. This real head model is subjected to various shock intensities under various head orientations. The head response under various shock intensities and different head orientations is studied and compared on the basis of concussive and axonal injury criterions available in the literature. Parametric studies over range of material properties are conducted and critical components and areas of head under blast loadings are identified.

Session: 2-9-1 Modeling of Brain Injury

Proceedings of the ASME 2010 International Mechanical Engineering Congress & Exposition
IMECE2010
November 12-18, 2010, Vancouver, British Columbia, Canada

IMECE2010-37949

COMPUTATIONAL SIMULATION OF THE DEFORMATION OF NEURONAL CELLS

Guoxin Cao
Department of Engineering Mechanics
University of Nebraska-Lincoln
Lincoln, NE, USA
gcao2@unl.edu

You Zhou
Center for Biotechnology
University of Nebraska-Lincoln
Lincoln, NE, USA
yzhou@unl.edu

Jeong Soon Lee
Department of Engineering Mechanics,
University of Nebraska-Lincoln
Lincoln, NE, USA
jlee12@unl.edu

Jung Yul Lim
Department of Engineering Mechanics,
University of Nebraska-Lincoln
Lincoln, NE, USA
jlim4@unl.edu

Namas Chandra
Department of Engineering Mechanics, University of Nebraska-Lincoln
Lincoln, NE, USA
nchandra2@unl.edu

EXTENDED ABSTRACT

ABSTRACT

A numerical simulation (finite element method (FEM)) is used to determine the local mechanical response of a neuron based on the real neuron geometry. The real 3D geometry of a neuron can be constructed from the 2D confocal image stack which is taken per micron along the thickness direction from the top surface of neuron to the substrate. By matching the simulated deformation of the neuron with the measured results from the confocal microscopy images, the relative strength of the neuron components can be determined based on the reverse analysis of FEM. Then, the neuron local mechanical response and the relationship between the local response and the global applied deformation can be obtained, which will be the first step of building the mechanical injury model of neuron.

INTRODUCTION

The mechanism of mild traumatic brain injury (mTBI) is directly related to the relationship between the mechanical response of neurons and their biological/chemical functions since the neuron is the main functional component of brain.[1] Therefore, understanding the mechanical response of neurons is an important first step to understand the mechanism of mTBI. Typically, the mechanical response of neurons is investigated based on the deformation of *in vitro* model, in which the substrate deformation is considered to be the deformation of neurons. However, neurons have the irregular shape and mainly include cell main body, neurite and axon which have highly different geometries and mechanical properties. Under the same global deformation (substrate deformation, e.g. substrate stretching), the different parts of a neuron might have the highly different local deformations. Therefore, it is important to understand the local mechanical response of neurons in order to get the accurate mechanical injury model of the neuron which describes the relationship between the neuron mechanical response and its function loss.

COMPUTATIONAL METHODS

A numerical simulation (finite element method (FEM)) can be used to determine the local mechanical response of a neuron based on the real neuron geometry. In FEM simulations, the real neuron geometry can be considered in both 2D and 3D. With the help of the software (Mimics),[2] the real 3D geometry of a neuron can be constructed from the 2D confocal image stack which is taken per micron along z-direction from the substrate to the top surface of neuron, as show in Figure 1. This 3D geometry can be further meshed in the finite element model, as shown in Figure 2. In FEM model, the neuron can be divided into three different regions: main cell body, neurite and axon, which have the different material properties. In the current work, all components of the neuron are modeled as both the elastic and the

viscoelastic materials. The standard linear model (SLS) is selected for the viscoelastic materials. Based on the scanning probe indentation, the mechanical properties of the neuron was reported from 480 to 1600Pa in the frequency range of 30~200Hz.[3] These values are considered to be the properties of the cell main body of a neuron since the indentation test is usually applied on the cell main body. The mechanical property ratio of the axon and the neurite to the cell main body can be firstly assumed to be one and then gradually increase or decrease to match their simulated deformation field with the experimental counterpart (confocal images of the deformed neuron).

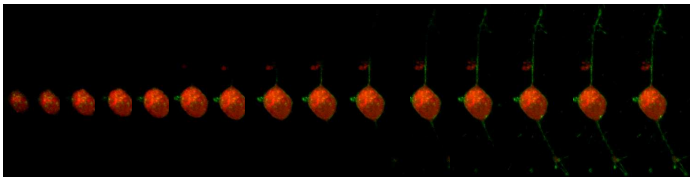

FIGURE 1. 2D confocal image stack of an isolated neuron (0.5μm between each image from the top surface to the substrate) .

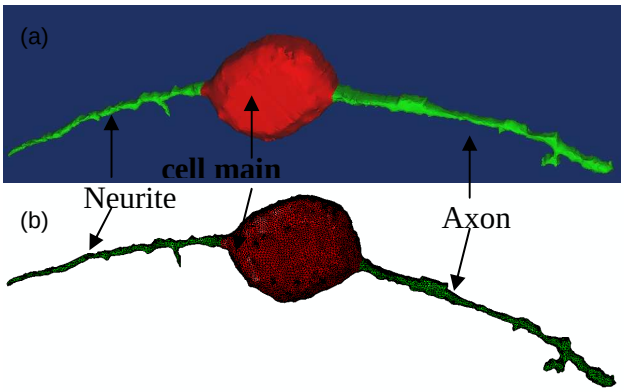

FIGURE 2. (a) 3D geometry of an isolated neuron created from 2D confocal image stack; (b) FEM mesh of 3D neuron structure.

EXPECTED RESULTS

In FEM simulations, the boundary condition of the neuron is selected similar to that used in the experiment. In the experiment, the neuron is assumed to be perfectly boned with the substrate, and, thus, the bottom of the neuron is clamped in the simulation. The uniaxial and equibiaxial stretch is applied on the neuron, respectively. The material properties of the neuron components are the set of properties which give the least difference between the simulated deformation field and the experimental counterpart.

CONCLUSIONS

The numerical simulation based on FEM can be used to determine the relative strength of the components of neurons: cell main body, axon and neurite by matching the simulated deformation field of a neuron and its experimental counterpart. Then, with those determined mechanical properties, the neuron local mechanical response and the relationship between the local response and the global applied deformation can be obtained, which will be the first step of building the mechanical injury model of neuron.

ACKNOWLEDGMENTS

The authors acknowledge the financial support provided by the U.S. Army Research Office (Project Monitor: Bruce Lamattina) for the project on "Army- UNL Center for Trauma Mechanics," contract number W911NF-08-1-0483.

REFERENCES

[1] Y. C. Chen, D. H. Smith and D. F. Meaney, J Neurotrauma 26 (2009) 861.
[2] http://www.materialise.com/materialise/view/en/2408037.
[3] Y. B. Lu, K. Franze, G. Seifert, C. Steinhauser, F. Kirchhoff, H. Wolburg, J. Guck, P. Janmey, E. Q. Wei, J. Kas and A. Reichenbach, Proceedings of the National Academy of Sciences of the United States of America 103 (2006) 17759.

Proceedings of the ASME 2010 International Mechanical Engineering Congress & Exposition
IMECE2010
November 12-18, 2010, Vancouver, British Columbia, Canada

IMECE2010-39447

MECHANICAL MODEL OF NEURONAL FUNCTION LOSS

Guoxin Cao
Department of Engineering Mechanics
University of Nebraska-Lincoln
Lincoln, NE, USA
gcao2@unl.edu

You Zhou
Center for Biotechnology
University of Nebraska-Lincoln
Lincoln, NE, USA
yzhou@unl.edu

Jeong Soon Lee
Department of Engineering Mechanics,
University of Nebraska-Lincoln
Lincoln, NE, USA
jlee12@unl.edu

Jung Yul Lim
Department of Engineering Mechanics,
University of Nebraska-Lincoln
Lincoln, NE, USA
jlim4@unl.edu

Namas Chandra
Department of Engineering Mechanics, University of Nebraska-Lincoln
Lincoln, NE, USA
nchandra2@unl.edu

EXTENDED ABSTRACT

INTRODUCTION

The mechanism of mild traumatic brain injury (mTBI) is directly related to the relationship between the mechanical response of neurons and their biological/chemical functions since the neuron is the main functional component of brain.[1] The hypotheses is that the external mechanical load will firstly cause the mechanical deformation of neurons, and then, when the mechanical deformation of neurons reaches to a critical point (the mechanical deformation threshold), it will initiate the chemical/biological response (e.g. neuronal function loss). Therefore, defining and measuring the mechanical deformation threshold for the neuronal cell injury is an important first step to understand the mechanism of mTBI.

Typically, the mechanical response of neurons is investigated based on the deformation of *in vitro* model, in which the neurons are cultured on the elastic substrate (e.g. PDMS membranes). The elastic membrane is deformed by the external load, e.g. equibiaxial stretching. The substrate deformation is considered to be the deformation of neurons since the substrate is several orders stiffer than the neurons and the neurons are perfectly bonded with the substrate. The fluoresce method is typically used to test the cell injury, e.g. the cell vitality and the neuron internal ROS level.[1, 2]

EXPERIMENTAL METHODS

Neuroblastoma cells from the SH-SY5Y cell line were used to measure the neuron injury threshold caused by the mechanical injury. The neurons were cultured as monolayers on the collagen-coated six-well FlexPlates (Flex, Hillsborough, NC, USA) in DMEM medium supplemented with 10% foetal calf serum (FCS). Cultures were maintained in humidified incubator (5% CO2, 37°C). Cells were seeded at the density of 5000 cells/cm^2. In order to make neurons fully differentiated, neurons were treated with 10μM retinoic acid (RA) over 4 days after 24hs cell culturing.

The cells were injured using Flexcell 5000 tension system (Flex, Hillsborough, NC, USA). The bottom of the FlexPlate wells are made by PDMS membrane with the thickness of 0.2mm. The membrane is stretched by a negative pressure pulse. The schematic of the cell stretching is shown in Figure 1. The cell deformation is same as the deformation of the PDMS membrane. In the neuron injury evaluation tests, initially an arbitrarily given deformation e.g. 30% will be applied on the cultured neuron monolayer, which should be strong enough to kill most of the PPDMS membrane. Then, the magnitude of applied strain will gradually be decreased until the injury thresholds are measured. The loading rate is about 0.01/s.

The nonlethal injury of neurons is interested since it might be directly related to the mTBI. The nonlethal

injury can be defined as follows. The mild injury means that the neuron can still survive for a period of time (24h) after unloading. The critical injury strain (ε_{cr}) is defined as the value of the applied external deformation beyond which the neuron will be mildly injured, while below which there will be no detectable injury. Since the neuron injury is determined based on the statistical results in current work, the applied deformation will cause about 80% of the neurons in each test (more than 200 neurons are counted) to have the detectable injury (nonlethal) defined to be the critical injury strain (ε_{cr}). The upper limit of the nonlethal injury of neurons (ε_{max}) is also defined. If the applied external deformation is beyond ε_{max}, the neuron will finally die. ε_{max} is defined as the value of the applied external deformation, causing about 30% of neurons to die in each test (more than 200 neurons are counted).

Dual fluorescence, live cell time-lapse confocal microscopy is carried out for identifying the neuron injury. Two different fluorescent reagents will be used: 1) a fluorescent ROS indicator, 2,7-dichlorofluorescin (DCF, 1 uM); 2) a HEPES-MEM containing 0.5 uM propidium iodide (PI, viability indicator); The stretched neurons will be loaded with both regents. An increase in DCF green fluorescence strength (usually in the cell cytoplasm) indicates the ROS reactions occurring as a result of a higher stress level of the cells in response to the external load (mechanical stretch and contraction). When cell viability changes as a result of alteration of membrane permeability in response to the mechanical stretch or contraction, the PI will enter the cells and binding DNAs/RNAs (proteins inside nucleus), resulting in red fluorescent nucleus structure.

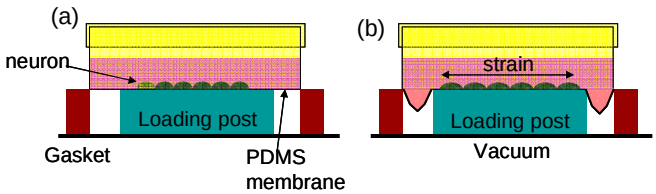

FIGURE 1. Schematic of neuron equibiaxial stretching.

RESULTS

Figure 2 shows the florescence images of SHSY5 neuronal cells. The cell density variation caused by the stretching is measured using the software Image J (NIH). Figure 3 shows the neuron density variation with ε =10%, 20% strain after 24h, and the control unit after 24h is also shown in Figure 3. The results show that the equibiaxial strain of 10% is the upper limit of the non-lethal injury (ε_{max}), which caused the death of about 30% neurons. The lower limit of the non-lethal injury (ε_{cr}) is about 5%, which is measured using the strength of DCF. The results of each well are based on the average values of 15 images.

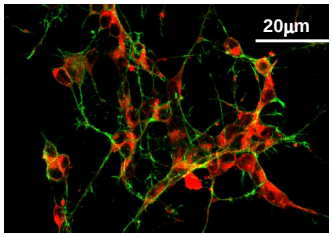

FIGURE 2. Fluorescence images of neuron monlayers.

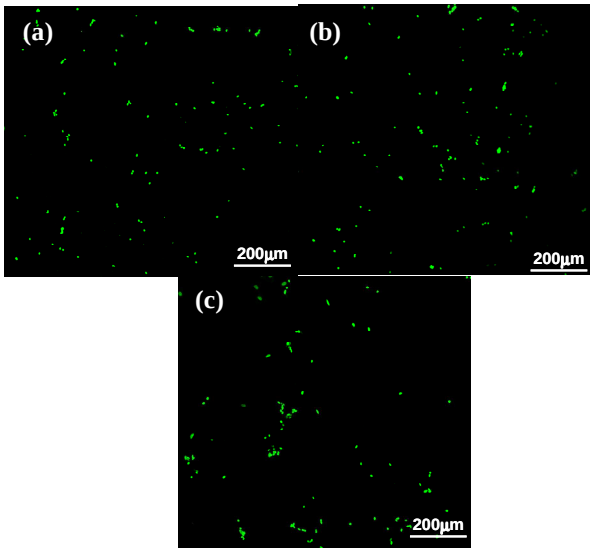

FIGURE 3. Fluorescence images of neuron density change, (a) control unit; (b) ε=10%; (c) ε=20%.

CONCLUSIONS

The nonlethal neuron injury is defined and measured based on the *In-Viro* cell model under the equibiaxial stretching. For SHSY5 neuronal cells, the upper limit of the non-lethal injury (ε_{max}), which caused the death of about 30% neurons. The lower limit of the non-lethal injury (ε_{cr}) is about 5%,

ACKNOWLEDGMENTS

The authors acknowledge the financial support provided by the U.S. Army Research Office (Project Monitor: Bruce Lamattina) for the project on "Army- UNL Center for Trauma Mechanics," contract number W911NF-08-1-0483.

REFERENCES

[1] Y. C. Chen, D. H. Smith, and D. F. Meaney, J Neurotrauma **26**, 861 (2009).

[2] B. Morrison, K. E. Saatman, D. F. Meaney, et al., Journal of Neurotrauma **15**, 911 (1998).

Evaluation of biological cell properties using dynamic indentation measurement

Guoxin Cao* and Namas Chandra†

Department of Engineering Mechanics, University of Nebraska-Lincoln, Lincoln, Nebraska 68588-0642, USA

(Received 18 May 2009; revised manuscript received 17 September 2009; published 26 February 2010)

Viscoelastic mechanical properties of biological cells are commonly measured using atomic force microscope (AFM) dynamic indentation with spherical tips. A semiempirical analysis based on numerical simulation is built to determine the cell mechanical properties. It is shown that the existing analysis cannot reflect the accurate values of cell elastic/dynamic modulus due to the effects of substrate, indenter tip size, and cell size. Among these factors, substrate not only increases the true contact radius but also interferes the indentation stress field, which can cause the overestimation of cell moduli. Typically, the substrate effect is much stronger than the other two influences in cell indentation; and, thus, the cell modulii are usually overestimated. It is estimated that the moduli can be overestimated by as high as over 200% using the existing analysis. In order to obtain the accurate properties of cells, correction factors that account for these effects are required in the existing analysis.

DOI: 10.1103/PhysRevE.81.021924 PACS number(s): 87.10.Kn

I. INTRODUCTION

There is a close relationship between the physical functions of cells and their mechanical behavior. For example, Cross *et al.* recently reported that the stiffness of metastatic cancer cells is 70% lower than that of healthy cells [1]; the heart muscle cells loss their contractility will cause the heart failure [2]; the traumatic brain injury (TBI) might be caused by the neuron death under the severe stretch [3]. Cells are typically considered as continuum materials and their mechanical behavior are described using continuum mechanics models. The parameters associated with models are considered to be the mechanical properties of cells which can be determined using experimental measurements. The most commonly used models are elastic and viscoelastic models based on which the elastic or dynamic modulus can be determined [4–15].

AFM is considered to be one of the best candidates for accurately measuring the load-displacement relationship of supersoft materials (~kPa) at a small scale. Thus, AFM is becoming one of the most popular ways to measure the cell properties [5–18]. Although the commercial nanoindenter has been widely used to measure the mechanical properties of materials at nanoscale or microscale, the applied force range of nanoindenter is still too high to accurately measure cell properties. For example, the applied force range for the Hysitron nanoindenter is from 30 nN to 10 N according to the menu [19].

The standard sharp AFM tip is likely to cause a very high stress concentration leading to highly nonlinear behavior. Also, the sharp tip may even tear the cell membrane. To avert these problems, a spherical tip is usually used instead of conventional tip in cell indentation [7,18]. In experiments, the radius of the indenter tip is usually chosen under 40 μm [5–7,9,18], compared to cells which are typically below 40 μm.

The cell is typically mounted on a substrate. Since the substrate is orders of magnitude stiffer than the cell by itself, the indentation force-displacement (P-δ) relationship will be influenced, especially for low cell thickness with deep indentation [5,7]. Though the substrate effect is minimal in shallow indentations, it is not practical to use shallow indentation to cells for the following reasons. In shallow indentations, it is highly difficult to accurately measure the contact area due to the surface roughness and very low stiffness of cells as well as the presence of adhesive force between the indenter tip and cell surface [10,20,21]. It is very important to understand and remove the substrate effect from the results of the AFM indentation measurement in order to obtain the true cell properties.

The substrate stiffening effect on the thin film indentation behavior has been widely investigated [22–24]. Based on the approaches initiated by Chen [23] and Tu *et al.* [24], Dimitriadis *et al.* introduce the correction terms into the Hertz contact model to correct the substrate stiffening effect on the elastic modulus of cell [25]. Mahaffy *et al.* [7] developed an analysis to obtain the viscoelastic properties of cells attached on the rigid substrate from the AFM dynamic indentation measurement. In this approach, the solution to the problem of cell indentation with substrate was assumed to be a series expansion of the standard Hertz elastic contact solution extended to linear viscoelastic materials. All of the above results and other reported cell properties measured using AFM indentation [6,9] are still based on the Hertz contact solution which is the solution derived for the semi-infinite elastic contact problem. In addition, the geometric characteristics of the cell (the cell diameter and thickness as well as the indenter tip size) are not considered, which may significantly affect the cell indentation response. For example, the substrate stiffening effect may not be just a function of cell thickness but also dependent on the indenter tip size and cell diameter. Therefore, it is highly necessary to establish an effective analysis to identify these effects and show the intrinsic properties of cell.

In this paper, the cell mechanical behavior is investigated using the semiempirical approach based on numerical simulations. In the simulations, the relationship between contact

*gcao2@unl.edu
†nchandra2@unl.edu

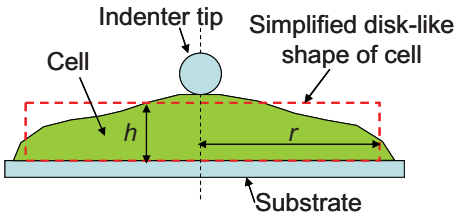

FIG. 1. (Color online) The schematic of cell indentation and simplified disklike shape.

radius and indentation displacement is established and the substrate effect is identified. The effects of indenter tip size, cell thickness, and cell radius on the indentation behavior are examined. The correcting factors are introduced into the existing indentation analysis; then cell properties can be more accurately determined. This study can help us to understand the intrinsic mechanical properties of cells and can provide a useful guideline for building the relationship between mechanical behaviors and biological functions.

II. COMPUTATIONAL METHODS

In the present work, the cell indentation behavior is studied using numerical simulations based on finite element modeling (FEM). After cells mounted on substrate, cells will expand themselves and the size along the normal direction of substrate is much less than the lateral size (as shown in Fig. 1). Cell geometry is typically described using two parameters: cell average radius r (along the lateral direction) and thickness h (along the normal direction of substrate) [4,6,10,11,26–29].

The cell is usually modeled as a continuous isotropic linear viscoelastic material. The standard linear solid (SLS) model is used to determine the dynamic modulus of cells as shown in Fig. 2. In the SLS model, the relaxation modulus is given by

$$E(t) = E_1 + E_2 e^{-t/\tau}, \tag{1}$$

where E_1 and E_2 are elastic modulus of springs and τ is the relaxation time, $\tau = \eta / E_2$, where η is the viscosity. The substrate and indenter tip are assumed to be rigid since they are usually several orders stiffer than the cell.

All FEM simulations are performed using commercial code ABAQUS v.6.8. Cells are geometrically simplified as two-dimensional (2D) axisymmetric disks. The spherical indenter tip is modeled as a 2D axisymmetric surface. The cell

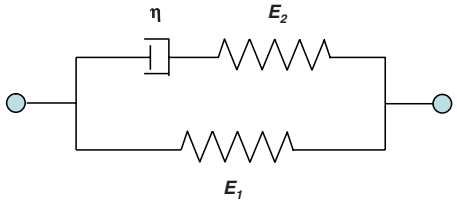

FIG. 2. (Color online) The standard linear solid model of viscoelastic material.

is represented by 25 000 four-node axisymmetric elements with reduced integration. The indenter tip radius (R) is selected from $1 \sim 15$ μm, which is commonly used in cell indentation [5,7]. The different cell radii (r) are selected as $r = 10$, 20 μm (typically less than 20 μm in radius). The different thicknesses (h) are selected as: $h = 5$, 10 μm (typically larger than 3 μm). In order to obtain an accurate contact radius, the size of surface elements in the contact area is set to less than 0.5% of the indenter tip radius. The Prony series coefficients of SLS model are $g = 0.3 \sim 0.9$ and $\tau = 1 \sim 10$ s as well as the instantaneous modulus range is $E_{\text{instant}} = 10 \sim 100$ kPa in FEM simulations. All degrees of freedom of nodes on the bottom of the cell are constrained to simulate the condition that the cell is fully adhered to the rigid substrate surface. All indentation simulations are performed based on displacement control. In order to examine the true substrate effect, the indentation displacement selected in the simulations coincide with the lowest experimentally applied value [5,7].

III. CONTACT RADIUS IN CELL INDENTATION

In indentation tests, the accuracy of the result is strongly influenced by the accuracy demonstrated in obtaining the indentation contact radius. In the following subsections, we will discuss the effects of geometric parameters (indenter tip radius R, cell thickness h and cell radius r) on the indentation contact radius in cell indentation and the corresponding physical mechanisms.

Based on dimensional analysis, the normalized contact radius can be described as a function of the normalized indentation displacement (δ/h), indenter tip radius (R/h), cell radius (r/R), and indentation force (P/Eh^2):

$$a/R = F(\delta/h, R/h, r/R, P/Eh^2).$$

The related geometric parameters are R, h, and r. Although it is reported recently that cells might be compressible [30,31], cells are commonly assumed as incompressible ($\nu \approx 0.5$). In the present work, the incompressible assumption is still used, and thus, ν is not considered as a variable in the present paper.

A. Effects of geometric parameters on contact radius

The variation in a_{num}/R with δ/h is shown in Figs. 3(a)–3(d), where a_{num} is the numerical solution of the contact radius. In the figure, the indenter tip radius $R = 1$, 15 μm, the cell radius $r = 10$, 20 μm and the cell thickness $h = 5$, 10 μm respectively. The FEM results are shown as thin lines (not smooth). For the sake of reference, the normalized Hertz contact radius, a_h/R, is shown as the dashed line. It is seen that when both R and h are small, the numerical solution (a_{num}) is very close to the Hertz solution (a_h) and a_{num} is not sensitive to r [the FEM result of the case with $r = 10$ μm is overlapped with the Hertz solution in Fig. 3(a)]. With the increase in R or h, a_{num} deviates from a_h and the deviation increases with δ/h. When both R and h are large, a_{num} increases with r. The effects of R, h, and r on a_{num} are coupled with each other. In addition, for a smaller R and a larger h,

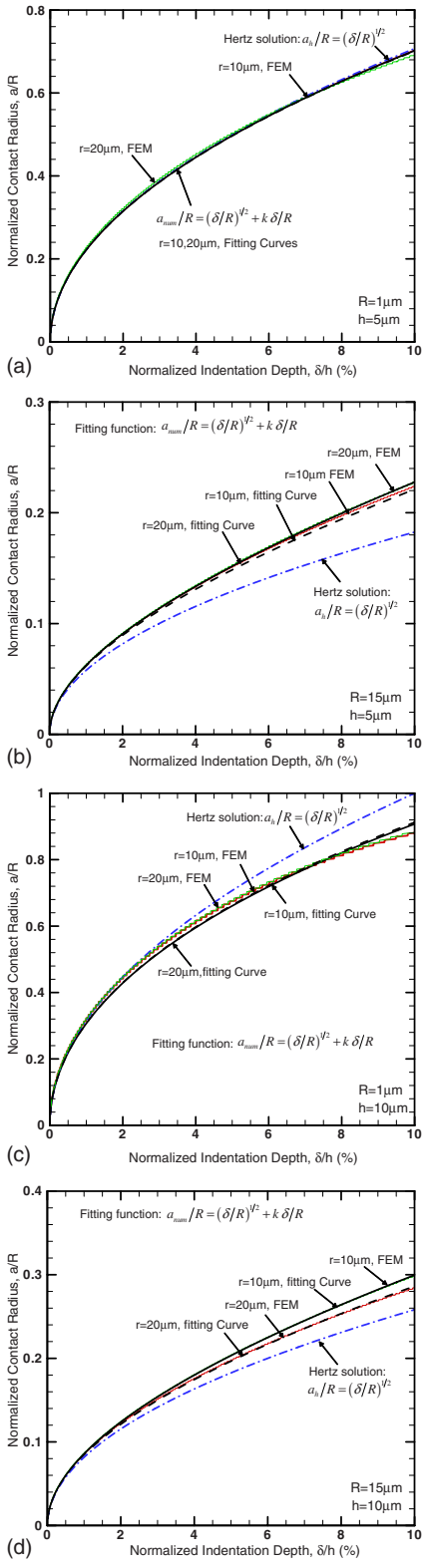

FIG. 3. (Color online) The relationship between normalized contact radius, a/R, and normalized indentation displacement, δ/h.

$a_{num}<a_h$; for a larger R and a smaller h, $a_{num}>a_h$.

For all cases in the present study ($1<R<15$ μm, $h=5,10$ μm, $r=10,20$ μm, $\delta/h<10\%$), the numerical solution of contact radius can be fitted as

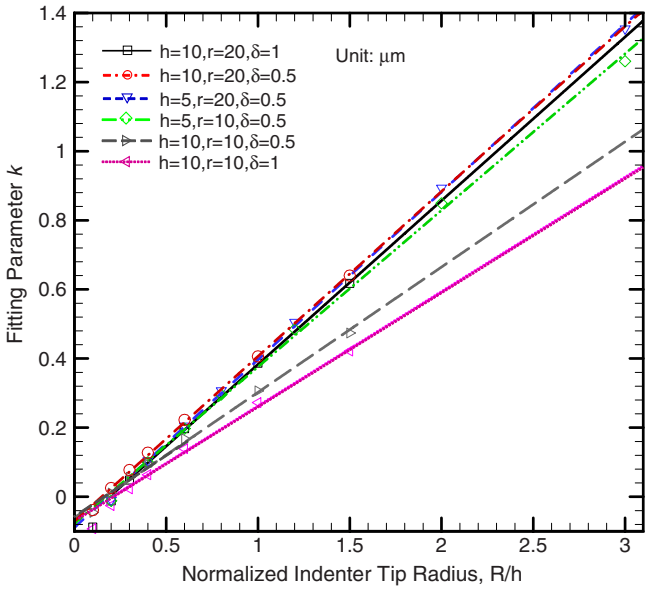

FIG. 4. (Color online) The fitting parameter k in Eq. (2).

$$\frac{a_{num}}{R}=\left(\frac{\delta}{R}\right)^{1/2}+k\frac{\delta}{R}, \tag{2}$$

where $k=k(R,h)$ is the fitting parameter, which also depends on the cell radius, r. The fitting curves of FEM results are shown as thick solid lines (smooth) in Figs. 3(a)–3(d). For all cases except for $R=1$ μm and $\delta=1$ μm, k can be fitted as $k=k_1+k_2R/h$, as shown in Fig. 4. The fitting parameter, k_1, is essentially a constant and $k_1\approx-0.083$. The fitting parameter $k_2\approx0.48$ for $r=20$ μm. However, k_2 decreases with the increase in δ or h when r reduces to 10 μm, as shown in the Fig. 4.

B. Basic mechanisms

It is evident that all geometric parameters R, h, and r will influence the contact radius due to nonlinear geometry, substrate, and boundary effects. Substitution of the expression of $k=k_1+k_2R/h$ into Eq. (2) leads to

$$a_{num}=(R\delta)^{1/2}+k_1\delta+k_2\frac{R}{h}\delta. \tag{3}$$

If $\delta\ll R$ and $\delta\ll h$, Eq. (3) converges to the Hertz solution. The second term, $k_1\delta$, in Eq. (3) is the geometric nonlinear correction term of the contact radius when the condition $\delta\ll R$ is not satisfied. The geometric nonlinear effect increases with the increase in δ or the decrease in R. In the present paper, the inclusion of the first-order term of δ is accurate enough to describe the geometric nonlinear effect. In fact, for very small R and large δ, higher-order terms of δ are required. For example, at $R=1$ μm and $\delta=1$ μm the first-order term of δ is not accurate enough (Fig. 4). Since k_1 is negative, the nonlinear geometric effect will reduce the contact radius compared with the Hertz solution. Generally, the nonlinear geometric effect can be reduced with a larger indenter tip size.

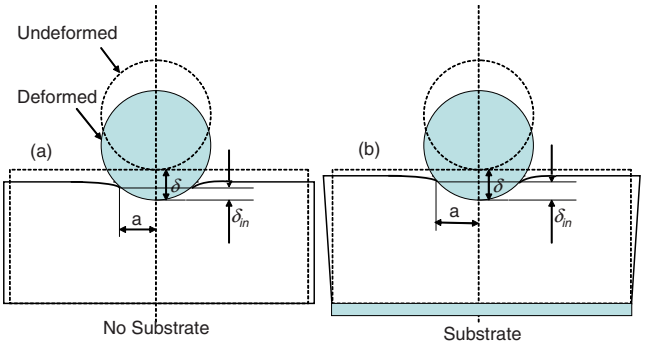

FIG. 5. (Color online) The schematics of cell indentation with and without substrate.

The third term in Eq. (3) can be considered as the substrate effect. Figure 5 shows the schematics of cell indentation with and without substrate. The cell compression in the thickness direction (introduced by the indentation) produces the cell stretching in the radial direction due to Poisson's effect. Both the compression and the stretching cause the penetration depth, δ_{in}, to be less than the displacement of indenter tip, δ. For example, $\delta \approx 2\delta_{in}$ in the Hertz solution. If a cell is fully adhered to a substrate, the substrate will constrain the bottom surface of the cell. Due to the small cell thickness, this constraint will reduce the cell stretching in the radial direction. This constraint effect increases the penetration depth, δ_{in}, under the same applied δ compared to the case without the substrate. Thus, the contact radius will be larger than the Hertz contact radius due to the substrate effect. The substrate effect on the contact radius increases with the decrease in h or increases with R.

The boundary effect reduces the contact radius by affecting the extent of the cell deformation along the radial direction caused by Poisson's effect. For given R, h, and δ, a smaller cell will deform easier than a larger cell along the radial direction due to the interaction between the free surface and the indentation stress field. This can be further supported by comparing the displacements along the radial direction, u_{11}, of both cells. The results show that u_{11} on the free surface of the smaller cell is much larger than u_{11} at the same radial position of the larger cell. The easier lateral deformation will reduce the penetration depth and thus reduce the contact radius. This effect increases with δ or R or decreases with the increase in r.

In summary, compared with the Hertz contact solution, the nonlinear geometry and the boundary effects reduce the contact radius, while the substrate effect increases the contact radius. With a large R/h ($R/h > 0.2$), the substrate effect is stronger than the nonlinear geometric and the boundary effects; and, thus, the contact radius is underestimated using Hertz contact radius. With a small R/h ($R/h < 0.2$), the substrate effect is smaller than the nonlinear geometrical effect (the boundary effect is very weak under this condition since R/r is very small); and, thus, the contact radius is overestimated using Hertz contact radius. Since typically $R/h > 0.2$ in the cell indentation, the contact radius is underestimated using the Hertz contact radius. This underestimation is smaller for a smaller R/h. In addition, the relationship between contact radius and indentation displacement is only dependent on the geometric parameters but not the material properties of cell (E, g, and τ). This has been validated using FEM simulations based on the different values of E, g, and τ ($E = 10 \sim 100$ kPa, $g = 0.3 \sim 0.9$, and $\tau = 1 \sim 10$ s).

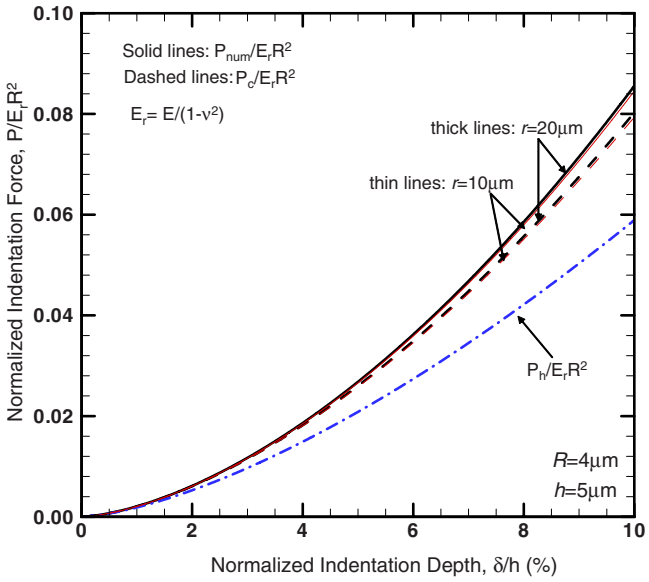

FIG. 6. (Color online) The relationship between the normalized indentation force and the normalized indentation displacement.

IV. EFFECT OF CONTACT RADIUS ON ELASTIC MODULUS

Since the Hertz solution cannot accurately describe the contact radius in cell indentation, in this section, we will discuss the effect of the Hertz contact radius on determining the cell modulus based on both elastic and viscoelastic material models. In order to obtain the correct cell modulus, the correcting factor for the Hertz contact radius is required.

A. Elastic materials

For a rigid spherical indenter, the indentation force is given by [32]

$$P = \frac{4}{3}\frac{E}{1-\nu^2}\frac{a^3}{R}, \tag{4}$$

where ν is the Poisson's ratio and E is the elastic modulus. If the deformation is infinitesimal, $\delta \ll R$, the contact radius is commonly approximated as the Hertz solution: $a \approx a_h = \sqrt{R\delta}$. Thus, the indentation force can be simplified as [32]

$$P_h = \frac{4}{3}\frac{E\sqrt{R}\delta^{3/2}}{1-\nu^2}. \tag{5}$$

The cell elastic modulus can be directly calculated from the measured $P_h \sim \delta$ relationship based on Eq. (5). One example of the indentation $P \sim \delta$ curve computed from the numerical simulation is shown in Fig. 6. P_{num} is the numerical solution of indentation force. The indentation force P_c calculated from Eq. (4) based on a_{num} and the Hertz solution of indentation force P_h calculated from Eq. (5) are also indicated as a

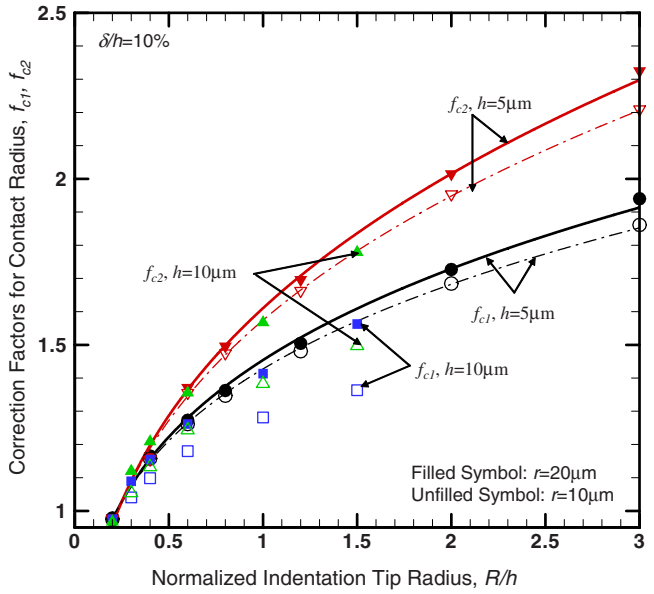

FIG. 7. (Color online) The correction factors to compensate for the effect from the Hertz contact radius on the cell elastic modulus, f_{c1} and f_{c2}.

dashed line and a dash-dot line, respectively. It can be seen that $P_{num} > P_c > P_h$. $P_{num} > P_h$ even at a small δ and $P_c \approx P_{num}$ when $\delta/h < 4\%$. With the increase in δ, P_{num} begins to deviate from P_c. This deviation is caused by the stress stiffening effect from substrate, which will be discussed in detail in the next section. The difference between P_c and P_h results from the inaccurate contact radius by the Hertz solution. Based on Eq. (4), the underestimation of contact radius will cause the overestimation of elastic modulus by a factor $f_{c1}=(a_{num}/a_h)^3$ as shown in Fig. 7.

The more popular way to determine the elastic modulus in nanoindentation tests is based on the contact stiffness $dP/d\delta$, which can be calculated by the first derivative of P with respect to δ in Eq. (5). The elastic modulus can be expressed as [33]

$$\frac{E}{(1-\nu^2)} = \frac{dP}{d\delta}\frac{1}{2a_h}, \tag{6}$$

where the contact stiffness $dP/d\delta$ can be measured from the P-δ curve in experiments. Since $dP/d\delta$ is easily measured in experiments (from the initial stage of the unloading curve slop), this way is more popular to measure the cell elastic modulus. However, if the contact radius is described by Eq. (2), Eq. (5) will change to

$$P = \frac{4}{3}\frac{E}{1-\nu^2}\frac{(\sqrt{R\delta}+k\delta)^3}{R}. \tag{7}$$

Based on the first derivative of P with respect to δ in Eq. (7), the elastic modulus is given by

$$\frac{E}{1-\nu^2} = \frac{dP}{d\delta}\left(\frac{4}{3}\sum_{m=1}^{4} n_m \frac{m+2}{2}(k)^{m-1}(R)^{1-m/2}(\delta)^{m/2}\right)^{-1}, \tag{8}$$

where $n_1=1$, $n_2=3$, $n_3=3$, $n_4=1$. When $m=1$, i.e., only the first term of the sequence in Eq. (8) is considered, then it reduces to Eq. (6). Thus, if $a_{num} > a_h$, then Eq. (6) can overestimate the elastic modulus by a factor f_{c2} in quasistatic indentation:

$$f_{c2} = \frac{2\xi(\delta)}{3a_h}, \tag{9}$$

$$\xi(\delta) = \sum_{m=1}^{4} \xi_m, \quad \xi_m = n_m \frac{m+2}{2}(k)^{m-1}(R)^{1-m/2}(\delta)^{m/2}. \tag{10}$$

f_{c2} is also shown in Fig. 7. It can be seen that $f_{c1} > f_{c2}$ for a given δ. Thus, Although Eqs. (5) and (6) are equivalent when $a \approx a_h = \sqrt{R\delta}$, Eq. (6) will cause a large overestimation for the elastic modulus than Eq. (5) when the contact radius is described using Eq. (2). In addition, E is not a constant but a function of the indentation displacement δ.

B. Viscoelastic materials

During the loading stage, the indentation force of viscoelastic material can be calculated using the correspondence principle: replacing the time-independent constant in Eq. (5) by the corresponding differential operators of the viscoelastic constitutive model [34].

$$P(t) = \frac{4}{3(1-\nu^2)R}\int_0^t E(s)\frac{d\{\sqrt{R\delta(t-s)}\}^3}{ds}ds. \tag{11}$$

In dynamic indentation with displacement control, the applied displacement profile is $\delta(t)=\delta_0+\Delta\delta\sin(\omega t)$. The indentation force can be also considered as a direct indentation force component superimposed with an oscillatory component $P(t)=P_0+\Delta P\sin(\omega t+\phi)$. The storage modulus and the loss modulus can be commonly determined based on the contact stiffness $(\Delta P/\Delta\delta)$ (Ref. [35]):

$$\frac{E'}{1-\nu^2} = \frac{1}{2a_h}\frac{\Delta P}{\Delta\delta}\cos\phi, \tag{12}$$

$$\frac{E''}{1-\nu^2} = \frac{1}{2a_h}\frac{\Delta P}{\Delta\delta}\sin\phi. \tag{13}$$

However, when the contact radius is described by Eq. (2), based on Eq. (7), Eq. (11) will change to

$$P(t) = \frac{4}{3(1-\nu^2)R}\int_0^t E(s)\frac{d\{\sqrt{R\delta(t-s)}+k\delta(t-s)\}^3}{ds}ds. \tag{14}$$

Then,

$$P(t) = \frac{4}{3}\frac{1}{1-\nu^2}\sum_{m=1}^{4} n_m (k)^{m-1}(R)^{1-m/2}\int_0^t E(s)\frac{d[\delta(t-s)]^{m/2+1}}{ds}ds, \tag{15}$$

where

$$\delta(t)^{m/2+1} = (\delta_0 + \Delta\delta \sin \omega t)^{m/2+1}$$

$$= \delta_0^{m/2+1} + \frac{m+2}{2}\delta_0^{m/2}\Delta\delta \sin \omega t + o(\Delta\delta),$$

$$m = 1 \sim 4. \tag{16}$$

Let

$$\xi(\delta_0) = \sum_{m=1}^{4} n_m \frac{m+2}{2}(k)^{m-1}(R)^{1-m/2}(\delta_0)^{m/2}. \tag{17}$$

Therefore, the oscillatory part is given by

$$\Delta P \sin(\omega t + \phi) = \frac{4}{3}\frac{1}{1-\nu^2}\xi(\delta_0)[E'(\omega)^2 + E''(\omega)^2]^{1/2}\Delta\delta \sin(\omega t + \phi), \tag{18}$$

$$\tan \phi = E''(\omega)/E'(\omega), \tag{19}$$

$$\frac{E'(\omega)}{1-\nu^2} = \frac{3}{4}\frac{\Delta P}{\Delta\delta}\frac{1}{\xi(\delta_0)}\cos \phi, \tag{20}$$

$$\frac{E''(\omega)}{1-\nu^2} = \frac{3}{4}\frac{\Delta P}{\Delta\delta}\frac{1}{\xi(\delta_0)}\sin \phi. \tag{21}$$

Similar to the analysis for elastic materials, if $a > a_h = \sqrt{R\delta}$, the conventional analysis [Eqs. (12) and (13)] will overestimate the complex modulus with the same factor:

$$f_{c2} = \frac{2\xi(\delta_0)}{3a_h(\delta_0)}. \tag{22}$$

From Eqs. (20) and (21), the dynamic modulus components are not only functions of the frequency of the oscillatory load, ω, but also functions of direct indentation displacement, δ_0. The phase difference, ϕ, between the indentation force and the indentation displacement is not affected by the correction of contact radius. The above results have been validated by FEM simulations with the SLS model ($g=0.3 \sim 0.9$, $\tau=1 \sim 10$ s, and $E_{\text{instant}}=10 \sim 100$ kPa) and actually f_{c2} does not depend on the parameters in SLS model.

V. NONLINEAR STRESS STIFFENING EFFECT

In this section, we will discuss the substrate stiffening effect on the cell modulus based on both elastic and viscoelastic material models. This effect will cause a significant overestimation of the cell elastic or dynamic modulus based on the Hertz solution. In order to get the accurate cell moduli, the correcting factor for the substrate stiffening effect is required for the conventional analysis.

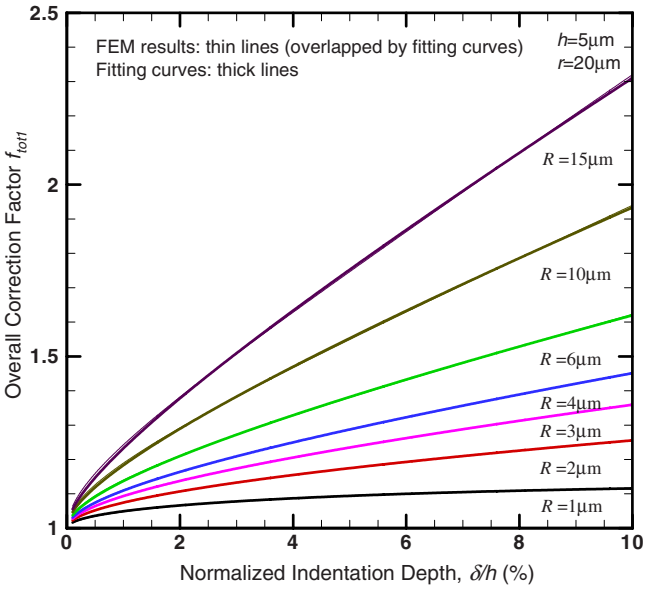

FIG. 8. (Color online) The relationship of the overall indentation correction factor f_{tot1} and normalized indentation depth, δ/h.

A. Elastic materials

The overall influences of both the underestimation of contact area and the stress stiffening effect from the substrate can be simply represented by a factor $f_{tot1}=P_{num}/P_h$ based on Eq. (4), which are shown as thin lines in Fig. 8. It can be seen that for all values of R, $f_{tot1} \approx 1$ at a very small δ/h; and f_{tot1} increases with δ/h and R. It shows that the elastic modulus is overestimated by a factor, f_{tot1}, based on Eq. (4) in the quasistatic indentation. The factor includes two components:

$$f_{tot1} = f_s + f_{c1} - 1, \tag{23}$$

where f_s is from the substrate stiffening effect and f_{c1} is from the underestimation of contact radius. For example, $f_{c1}=1.92$, $f_{tot1}=2.3$ at $\delta/h=10\%$, and, thus, $f_s=1.38$ for the cell with $h=5$ μm, $R=15$ μm, and $r=20$ μm. This means that the overall overestimation of the elastic modulus is 130%, wherein the underestimation of the contact radius contributes to about 92%, and the rest from the substrate stiffening effect is about 38%.

Figure 9 shows the variation in f_{tot1} with R/h at $\delta/h=10\%$. f_{tot1} increases with R/h. With a larger cell radius $r=20$ μm, f_{tot1} is essentially insensitive to h. Further, with a smaller thickness $h=5$ μm, f_{tot1} is insensitive to r; but the effect of r becomes larger with h. The effect of r on f_{tot1} arises mainly from the influence of f_{c1}, which can be reduced by selecting smaller R/h.

For a given cell radius, r, f_{tot1} can be fitted as a function:

$$f_{tot1} = P_{num}/P_h = 1 + b(\delta/h)^{1/2} + c(\delta/h). \tag{24}$$

The fitting results of the cells with $r=20$ μm and $h=5$ μm are shown as thick lines in Fig. 8 (they are overlapped with the FEM results). The coefficients b and c in Eq. (24) can be fitted as functions of R/h: $b=b_1(R/h)^{1/2}+b_2$, $c=c_1R/h+c_2$, as shown in Fig. 10. For cells with $h=5$ μm,

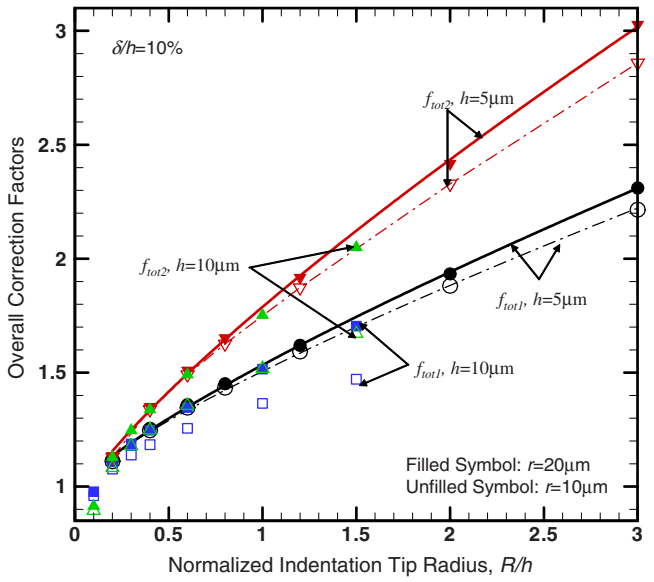

FIG. 9. (Color online) The comparison between the overall correction factors, f_{tot1} and f_{tot2} of the elastic modulus.

these constants can be found as $b_1 \approx 0.73$, $b_2 \approx 0.27$, and $c_1 \approx 3.0$, $c_2 \approx -0.9$.

P_{num} can be expressed as that P_h multiplied by a function: $g(\delta/h)=1+b(\delta/h)^{1/2}+c(\delta/h)$, which represents the effect of geometric parameters (small R, large δ, and low h with substrate). Thus,

$$P_{num} = \frac{4}{3}\frac{E\sqrt{R}\delta^{3/2}}{1-\nu^2} g\left(\frac{\delta}{h}\right). \tag{25}$$

Then based on the contact stiffness, $dP_{num}/d\delta$, Eq. (6) will change to

$$\frac{E}{1-\nu^2} = \frac{3}{4}\frac{dP_{num}}{d\delta}[\zeta(\delta)]^{-1}. \tag{26}$$

$$\zeta(\delta) = R^{1/2}\sum_{m=1}^{3} l_m \frac{m+2}{2}\delta^{m/2}h^{(1-m)/2}, \tag{27}$$

where $l_1=1$, $l_2=b$, $l_3=c$. Therefore, if $a > a_h=\sqrt{R\delta}$ and with the substrate effect, The more popular method based on the contact stiffness [Eq. (6)] will overestimate the elastic modulus by a factor f_{tot2}:

$$f_{tot2} = \frac{2\zeta(\delta)}{3a_h(\delta)}. \tag{28}$$

It can be seen that $f_{tot2} > f_{tot1}$, as shown in Fig. 9. The overestimation of elastic modulus can be as high as 200% based on the more popular way [Eq. (6)], wherein the underestimation of a contributes about 130%, as shown in Fig. 7, and the rest arising from the stress stiffening effect.

B. Viscoelastic materials

For the viscoelastic materials with substrate effect, the components of complex modulus are given by

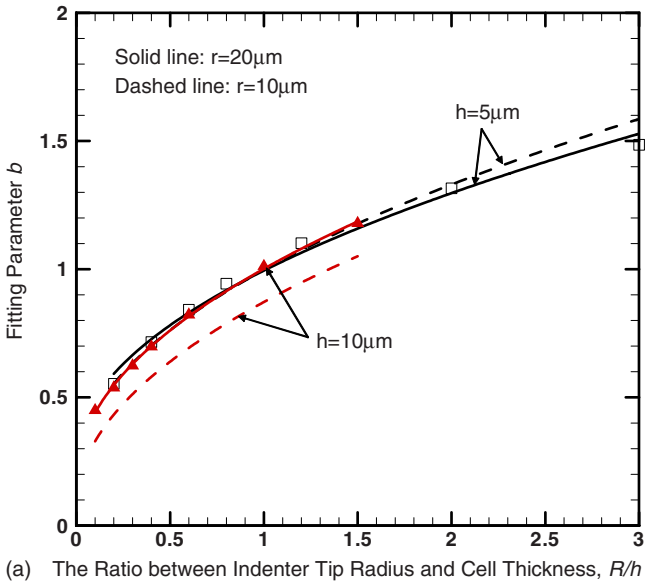

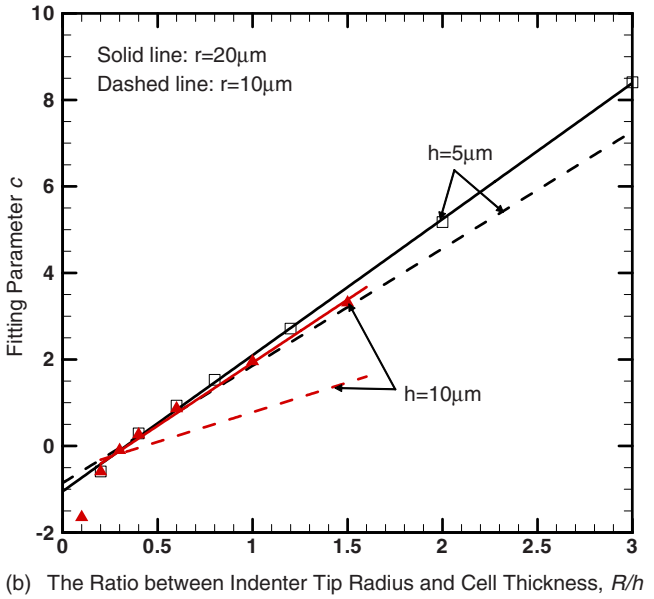

FIG. 10. (Color online) The fitting parameters b and c in Eq. (24).

$$\frac{E'(\omega)}{1-\nu^2} = \frac{3}{4}\frac{\Delta P}{\Delta\delta}\frac{1}{\zeta(\delta_0)}\cos\phi, \tag{29}$$

$$\frac{E'(\omega)}{1-\nu^2} = \frac{3}{4}\frac{\Delta P}{\Delta\delta}\frac{1}{\zeta(\delta_0)}\cos\phi, \tag{30}$$

$$\tan\phi = E''(\omega)/E'(\omega), \tag{31}$$

where $\zeta(\delta_0)=R^{1/2}\sum_{m=1}^{3} l_m\frac{m+2}{2}\delta_0^{m/2}h^{(1-m)/2}$. Similar to elastic materials, if $a > a_h=\sqrt{R\delta}$ and with the substrate effect, Eqs. (12) and (13) will overestimate the complex modulus by the same factor:

$$f_{tot2} = \frac{2\zeta(\delta_0)}{3a_h(\delta_0)}. \quad (32)$$

From Eqs. (29)–(31), it can be seen that the phase difference is not affected by the substrate effect; and the components of the intrinsic dynamic modulus can be provided by Eqs. (29) and (30). The above results have been validated using FEM simulations with the SLS model ($g=0.3\sim0.9$, $\tau=1\sim10$ s, and $E_{\text{instant}}=10\sim100$ kPa) and actually the substrate effect is not dependent on the values of g and τ used in the SLS model.

VI. SUMMARY AND CONCLUSIONS

In this work, a semiempirical analysis is built based on FEM simulations to determine the cell mechanical properties from the spherical AFM indentation response. The results show that the existing indentation analysis can overestimate the dynamic modulus by as high as 200% in some cases. The overestimation is mainly caused by the inaccurate determination of the indentation contact radius and the improper accounting of the substrate effect. The effects of inaccurate contact radius and substrate depend on the geometric parameters: indentation tip radius, cell radius, and cell thickness but do not depend on the material properties (E, g, and τ). Correction factors have been proposed in this work that relate the geometric parameters to the mechanical properties in quasistatic and dynamic indentation tests.

The inaccurate determination of the contact radius is caused by the nonlinear geometric, finite boundary, and substrate effects. Substrate not only affects the value of the contact radius but also stiffens the cell. The substrate effect increases with an increase in indenter tip radius, indentation displacement, or a decrease in cell thickness. The nonlinear geometric effect increases with a decrease in indenter tip radius. The boundary effect reduces with cell thickness or/and indenter tip radius. When the indenter tip radius is small, the nonlinear effect is dominant compared to substrate and boundary effects. When the tip radius is large, the substrate effect is dominant. To remove these effects, the correction factors f_{tot1} and f_{tot2} are induced, composed of the contact area correction factor and the stress stiffening factor. They increase with the increase in R/h or the decrease in h. For a small h, the correction factors are not sensitive to r; for a large h, they decrease with r.

ACKNOWLEDGMENTS

The authors acknowledge the financial support provided by the U.S. Army Research Office for the project on "Army-UNL Center for Trauma Mechanics," Contract No. W911NF-08-1-0483. The authors also thank Dr. Jiashi Yang and Dr. M. Negahban at UNL for many useful discussions.

[1] S. E. Cross, Y. Jin, J. Rao *et al.*, Nat. Nanotechnol. **2**, 780 (2007).
[2] Y. C. Fung, *Biomechanics: Mechanical Properties of Living Tissues* (Springer, New York, 1993).
[3] B. Morrison, K. E. Saatman, D. F. Meaney *et al.*, J. Neurotrauma **15**, 911 (1998).
[4] C. T. Lim, E. H. Zhou, and S. T. Quek, J. Biomech. **39**, 195 (2006).
[5] Y. B. Lu, K. Franze, G. Seifert *et al.*, Proc. Natl. Acad. Sci. U.S.A. **103**, 17759 (2006).
[6] V. Lulevich, R. Zink, H.-Y. Chen *et al.*, Langmuir **22**, 8151 (2006).
[7] R. E. Mahaffy, S. Park, E. Gerde *et al.*, Biophys. J. **86**, 1777 (2004).
[8] P. Carl and H. Schillers, Pflugers Arch. Eur. J. Physiol. **457**, 551 (2008).
[9] J. C. Hansen, J. Y. Lim, L.-C. Xu *et al.*, J. Biomech. **40**, 2865 (2007).
[10] S. Gupta, F. Carrillo, M. Balooch *et al.*, J. Mater. Res. **20**, 1979 (2005).
[11] T. Ohashi, Y. Ishii, Y. Ishikawa *et al.*, Biomed. Mater. Eng. **12**, 319 (2002).
[12] F. Rico, P. Roca-Cusachs, N. Gavara *et al.*, Phys. Rev. E **72**, 021914 (2005).
[13] T. G. Kuznetsova, M. N. Starodubtseva, N. I. Yegorenkov *et al.*, Micron **38**, 824 (2007).
[14] M. Radmacher, Methods Cell Biol. **83**, 347 (2007).
[15] C. Callies, P. Schöon, I. Liashkovich *et al.*, Nanotechnology **20**, 175104 (2009).
[16] E. J. Koay, A. C. Shieh, and K. A. Athanasiou, J. Biomech. Eng. **125**, 334 (2003).
[17] Q. S. Li, G. Y. H. Lee, C. N. Ong *et al.*, Biochem. Biophys. Res. Commun. **374**, 609 (2008).
[18] R. E. Mahaffy, C. K. Shih, F. C. MacKintosh *et al.*, Phys. Rev. Lett. **85**, 880 (2000).
[19] http://www.hysitron.com/page_attachments/0000/0621/TI_950_TriboIndenter_information.pdf
[20] Y. T. Cheng and C. M. Cheng, Mater. Sci. Eng. R. **44**, 91 (2004).
[21] S. Gupta, F. Carrillo, C. Li *et al.*, Mater. Lett. **61**, 448 (2007).
[22] B. Oommen and K. J. Van Vliet, Thin Solid Films **513**, 235 (2006).
[23] W. T. Chen, Int. J. Eng. Sci. **9**, 775 (1971).
[24] Y.-O. Tu and D. C. Gazis, J. Appl. Mech. **31**, 659 (1964).
[25] E. K. Dimitriadis, F. Horkay, J. Maresca *et al.*, Biophys. J. **82**, 2798 (2002).
[26] I. Kang, D. Panneerselvam, V. P. Panoskaltsis *et al.*, Biophys. J. **94**, 3273 (2008).
[27] H. Karcher, J. Lammerding, H. Huang *et al.*, Biophys. J. **85**, 3336 (2003).
[28] C. Y. Zhang and Y. W. Zhang, Philos. Mag. **87**, 3415 (2007).
[29] C. Y. Zhang, Y. W. Zhang, and K. Y. Zeng, J. Mater. Res. **19**, 3053 (2004).
[30] G. Ofek, D. C. Wiltz, and K. A. Athanasiou, Biophys. J. **97**, 1873 (2009).
[31] W. R. Trickey, F. P. T. Baaijens, T. A. Laursen *et al.*, J. Bio-

mech. **39**, 78 (2006).
[32] I. N. Sneddon, Int. J. Eng. Sci. **3**, 47 (1965).
[33] G. M. Pharr, W. C. Oliver, and F. R. Brotzen, J. Mater. Res. **7**, 613 (1992).
[34] E. H. Lee and J. R. M. Radok, ASME J. Appl. Mech. **27**, 438 (1960).
[35] E. G. Herbert, W. C. Oliver, and G. M. Pharr, J. Phys. D **41**, 074021 (2008).

16th US National Congress of Theoretical and Applied Mechanics
June 27 - July 2, 2010, State College, Pennsylvania, USA

USNCTAM2010-1026

MODELING SHOCK RESPONSE OF HELMETED HEAD USING FLUID STRUCTURE INTERACTION

SHAILESH GANPULE
University of Nebraska Lincoln
Department of Engineering Mechanics
Lincoln, Nebraska 68588-0526, USA
sgganpule@gmail.com

LINXIA GU
University of Nebraska Lincoln
Department of Mechanical Engineering
Lincoln, Nebraska 68588-0656, USA
lgu2@unlnotes.unl.edu

NAMAS CHANDRA
University of Nebraska Lincoln
Department of Engineering Mechanics
Lincoln, Nebraska 68588-0526, USA
nchandra2@unlnotes.unl.edu

INTRODUCTION

Blast induced traumatic brain injury (bTBI) is signature injury in recent combat scenarios involving improvised explosive devices (IEDs). The exact mechanisms of bTBI are still unclear and protective role of helmet and body armor is often questioned [1-3]. High Fidelity finite element models involving fluid structure interaction are built in order to understand effectiveness of helmet in mitigating early time blast induced mild traumatic brain injury.

METHODOLOGY

Two dimensional plane strain finite element models of helmet-head under shock loading are studied to compare effectiveness of helmet. Figure 1 shows the configuration of setup.

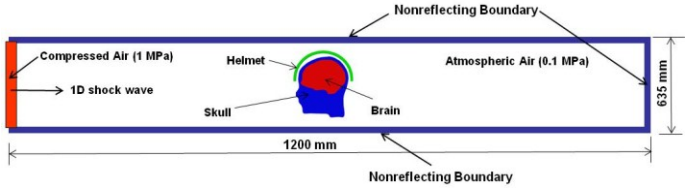

Figure 1 : Simulation setup. Frontal blast is simulated.

Our blast scenarios are simulated by first positioning the head model in an atmosphere of air at ambient conditions as shown in Fig.1. Shock wave is generated by releasing high pressure compressed air into atmospheric air at time equal to zero. The pressure and thickness of compressed air domain is selected so as to generate nonlethal blast wave. The structure of this blast wave is illustrated in Fig. 2.

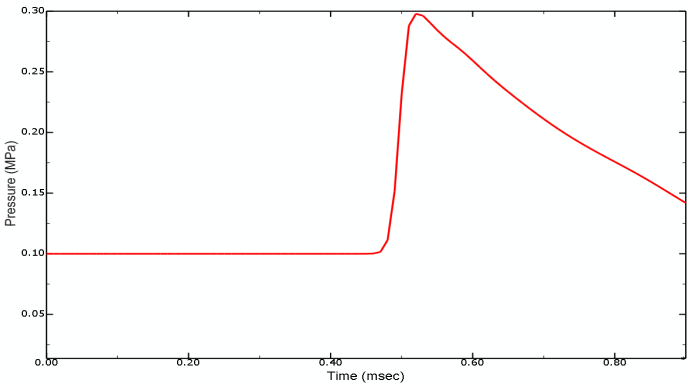

Figure 2 : Wave form of approximated air blast structure of 0.3 MPa magnitude

Our head model consists of skull , facial bones , neck bones and brain. We have used same material properties for skull , facial bones and neck bones hence we do not distinguish them as separate component. skull , facial bones and neck bones together will be referred as 'skull' henceforth. The geometry of these components is obtained by segmentation of MRI dataset available from visible human project of the National Library of Medicine [4]. Since we are interested in 2-dimensioanl head model , the central slice of MRI dataset is chosen. These geometries are imported into finite element software [5] and then meshed to generate 2-dimensional plain strain finite element head model. 2-dimensioanl geometries were selected so that the analysis would not be overly complex and prohibitively expensive.

The brain tissue is modeled as linear, isotropic, viscoelastic material with properties adopted from Taylor et al.[2]. Standard Linear Solid (SLS) model is used to characterize shear response. The skull is modeled as linear, elastic, isotropic materials based on material models suggested in the literature

[6-9]. The Kevlar helmet is modeled as hollow hemiellipsoid with a constant thickness and offset from the skull as described by Reynosa [10], with transversely isotropic elastic material properties given by Aare and Keliven [11]. Dry air, the medium through which blast wave propagates is modeled as ideal gas equation of state.

RESULTS

We have studied how helmets influence the blast-induced mechanical loads in the brain. Helmeted and non helmeted response is compared on the basis of pressure in the helmet cranium subspace , contact pressure on the outer surface of the skull and pressure and shear stresses (mises) in the various regions of the brain. Figure 3 shows pressure at air cranium (skull) interface. The blast pressure increases about 3.6 times due to impedance mismatch.

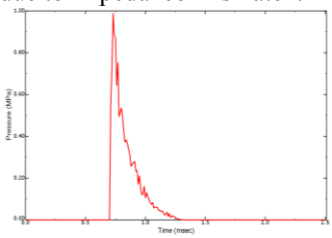

Figure 3: Blast pressure at air skull interface

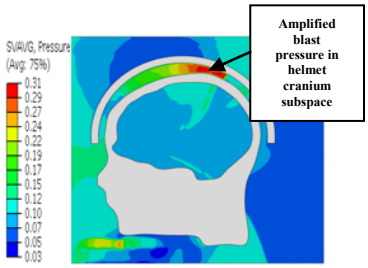

Figure 4: Uderwash effect of the helmet

Figure 4 is from a blast simulation of a head with helmet. The 1.3 cm gap between helmet and head allows the blast wave to wash under the helmet. When this ‘‘underwash’’ occurs, geometric focusing of the blast wave causes the pressures under helmet cranium subspace to exceed those outside the helmet . This is in turn causes additional loads on the top portion of the skull where the ‘‘underwash’’ effect is most dominant. Underwash effect is however not dominant in front regions of the skull. Figure 5 (a) and (b) compares pressure in top and front regions of helmet cranium subspace. The pressure in helmet cranium subspace is transferred to skull and brain. Figure 6 (a) and 6 (b) shows pressure in top and front regions of the brain respectively. As seen from these figures helmet reduces the pressure in frontal region of the brain however it increases the pressure in top regions of brain due to "underwash" effect occurring in top regions of helmet cranium subspace. Similar trend is observed for shear stress (mises) in the brain and contact pressures on the outer surface of the skull.

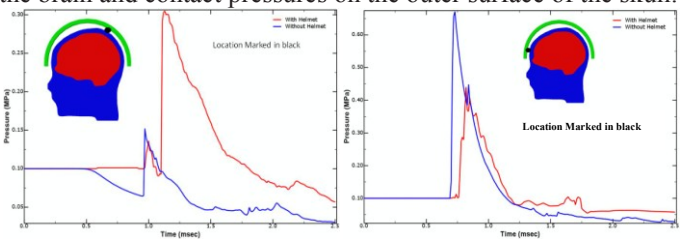

Figure 5: Pressure history of marked locations of helmet cranium subspace

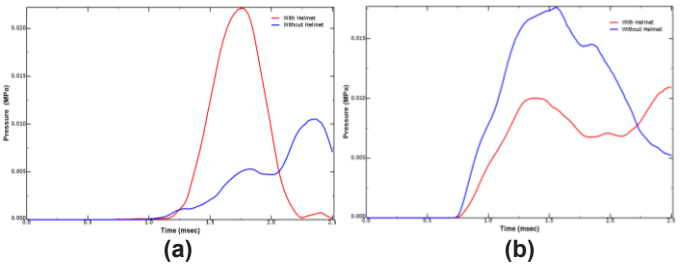

Figure 6: Average pressure in the brain. (a) Top Region (b) Front Region

CONCLUSIONS

We have conducted blast simulations to understand response of head with protection of helmet. Head was subjected to 0.3 MPa blast overpressure. Our simulation shows peak overpressure rise of about 333.33 % at fluid solid interface. We have simulated 1.3 cm gap scenario between head and helmet. Helmet protects frontal region of brain as it attenuates shock intensity reaching the frontal side of head. On the other hand, helmet has adverse effect in protecting top regions of the head due to 'underwash' effect in top regions of helmet cranium sub space.

REFERENCES

[1] Moore D.F. et al, 2009, "Computational biology - Modeling of primary blast effects on the central nervous system," NeuroImage, 47(Suppl.2), pp. T10-T20.

[2] Taylor, P.A., Ford, C.C., 2008, "Modeling and Simulation of Blast-Induced, Early-Time Intracranial Wave Physics leading to Traumatic Brain Injury," Sandia Report, SAND2008-0330.

[3] Moss, W.C., King, M.J., Blackman, E.G., 2009, " Skull Flexure from Blast Waves: A Mechanism for Brain Injury with Implications for Helmet Design, " Physical Review Letters, 103, 108702.

[4] National Institutes of Health, 2007, “The Visible Human Project,” National Library of Medicine, http://www.nlm.nih.gov/research/visible/ visible_human.html

[5] Abaqus 6.9-1, 2009, Providence, Rhode Island, USA.

[6] McElhaney, J.H., Fogle, J.L., Melvin, J.W., Haynes, R.R., Roberts, V.L., Alem, N.M., 1970, "Mechanical Properties of Cranial Bone," J. Biomechanics, 3, pp.495-511.

[7] Barber, T., Brockway, J., Moffa, C., 1970, " Static Compression Testing of Specimens from an Embalmed Human Skull," Texas Reports on Biology and Medicine, 28, pp.497-508.

[8] Schueler, F., Zimmer, G., Min, J., Mattern, R., 1994, " Assessment of Mechanical Properties of the Human Skull-Cap through Basic Biomechanical Tests and Quantitative Computed Tomography (QCT), " Proceeding of the International Research Council On Biokinetics of Impact (IRCOBI), pp.23-37.

[9] Nishimoto, T., Murakami, Sh., Abe, T., Ono, K., 1995, "Mechanical Properties of Human Cranium and Effect of Cranial Fractures on Extradural Hematoma," Nippon Kikai Gakkai Ronbunshu A Hen, Transactions of the Japan Society of Mechanical Engineers, Part A, 61(591), pp. 2386-2392.

[10] M.A. Reynosa, 1999, "The Personnel Armor System Ground Troops (PASGT) Helmet," Schiffer Military History, Atglen, PA.

[11] Aare and S. Kleiven, 2007, Int. J. Impact Eng., 34, 596-608.